AD_____

Award Number: DAMD17-97-1-7251

TITLE: BCL-2, Ca, and Apoptosis in Breast Cancer

PRINCIPAL INVESTIGATOR: Terry Machen, Ph.D.

CONTRACTING ORGANIZATION: The University of California, Berkeley
Berkeley, California 94720

REPORT DATE: August 2000

TYPE OF REPORT: Final

PREPARED FOR: U.S. Army Medical Research and Materiel Command
Fort Detrick, Maryland 21702-5012

DISTRIBUTION STATEMENT: Approved for Public Release;
Distribution Unlimited

REPORT DOCUMENTATION PAGE

OMB No. 0704-0188

1. AGENCY USE ONLY (Leave blank)	2. REPORT DATE	3. REPORT TYPE AND DATES COVERED
	August 2000	Final (1 Aug 97 - 31 Jul 00)

4. TITLE AND SUBTITLE
BCL-2, Ca, and Apoptosis in Breast Cancer

5. FUNDING NUMBERS
DAMD17-97-1-7251

6. AUTHOR(S)
Terry Machen, Ph.D.

7. PERFORMING ORGANIZATION NAME(S) AND ADDRESS(ES)
The University of California, Berkeley
Berkeley, California 94720

E-MAIL:
machen@socrates.berkeley.edu

8. PERFORMING ORGANIZATION REPORT NUMBER

9. SPONSORING / MONITORING AGENCY NAME(S) AND ADDRESS(ES)
U.S. Army Medical Research and Materiel Command
Fort Detrick, Maryland 21702-5012

10. SPONSORING / MONITORING AGENCY REPORT NUMBER

11. SUPPLEMENTARY NOTES

12a. DISTRIBUTION / AVAILABILITY STATEMENT
Approved for public release; distribution unlimited

12b. DISTRIBUTION CODE

13. ABSTRACT *(Maximum 200 Words)*

Apoptosis of non-transformed mammary cells 31EG4 was associated with an apparent 50% reduction of the ER Ca store, and Ca entry through Ca channels was also reduced (imaging microscopy). Deconvolution microscopy showed that degenerating nuclei in apoptosing cells contained regions of very high Ca, likely due to the accumulation of endoplasmic reticulum within lobed nuclei. Confluent monolayers also absorbed Na through apical ENaC (Na channels) and secreted Cl through apical CFTR (Cl channels); fluid was absorbed or secreted depending on the relative activities of these channels and the properties of tight junctions. Fluid transport could contribute to fluid accumulation in breast cysts. It was expected that dissolution of tight junctions would need to occur in a very coordinated way during apoptosis. Control cells had a predicted array of F-actin, ZO-1 and occludin. Mechanical disruption of the monolayer caused cells adjacent to the wounds to lose the organized actin/ZO-1/occludin-containing junctions in an organized sequence, while junctions were retained between adjacent cells. Following migration of cells to fill the wound, tight junctions rapidly reformed in a stereotypical sequence at points of initial contact between cells from opposite sides of the wound using cytosolic pools of proteins.

14. SUBJECT TERMS	15. NUMBER OF PAGES
Breast Cancer, apoptosis, calcium signaling, tight junctions, CFTR, ENaC	65
	16. PRICE CODE

17. SECURITY CLASSIFICATION OF REPORT	18. SECURITY CLASSIFICATION OF THIS PAGE	19. SECURITY CLASSIFICATION OF ABSTRACT	20. LIMITATION OF ABSTRACT
Unclassified	Unclassified	Unclassified	Unlimited

Table of Contents

INTRODUCTION

An attempt was made to assess the role of Bcl-2 in control of mitochondria and endoplasmic reticulum Ca transport and apoptosis in breast cancer was investigated. The general hypothesis was that Bcl-2 played a role in Ca homeostasis of the cells, and this role was crucial to the activation of apoptosis.

BODY

Technical Objectives (TO)

TO #1 Task 1. Completed, but G-418 killing curve was not completed since these cells were insensitive to this drug. We completed a hygromycin killing curve in preparation for attempting to transfect the cells with the bcl-2 plasmid.
TO #1 Task 2. Not completed due to the inability to generate a stable cell line expressing bcl-2 gene.
TO #1 Task 3. Bcl-2 western blots and immunofluorescence were performed on 31EG4 cells expressing the bcl-2 plasmid, but there were only a few cells expressing the protein. Confocal observations of bcl-2 expressing cells were not completed due to the inability to generate a stable cell line.

TO #2 Task 1. Completed time course of apoptosis induction with staurosporine, mitomycin and collagenase IV, indentifying morphological transformations in living cells.

TO #3 Task 1. Ca in the cytosol, Ca permeability of the plasma membrane and Ca content of the ER was evaluated indirectly from measurements of cytosolic Ca during control and during late stage apoptosis.
TO #3 Task 2. Bcl-2 transfections were not completed, so this objective was not completed.
TO #3 Task 3. Mitochondrial function in terms of Ca transport was not completed.

1. Stable transfection of 31EG4 cells with the bcl-2 gene.

Although we tried many different protocols for transfecting the normal, untransformed mouse cells with the bcl-2 plasmid, it proved impossible to generate a stable cell line. This work was described in a previous report. Our inability to generate a stable cell line may have been due to the effects of the bcl-2 gene on normal cell replication. We decided to work instead on the other aims.

2. Determine the time course of apoptosis of 31EG4 cells during activation with a number of different agents in control and bcl-2-transfected cells.

2a. Time course of apoptosis. We tested the well known activators staurosporine (nonspecific protein kinase inhibitor), mitomycin C (the DNA-alkylating agent), collagenase IV (degrades the basement membrane produced by the 31EG4 cells) and thapsigargin (inhibitor of the Ca^{2+} pump responsible for moving Ca^{2+} from the cytosol into intracellular stores). Apoptosis occurred with a characteristic time course beginning at approximately 16 hours and continuing during the next 32 hrs.

2b. Morphology of apoptosis. Staining with both permeant nuclear dyes (SYTO) and cytosolic and ER-localized dyes (fura-2) showed the characteristic shrinkage of the cells and blebbing was preceded by membrane phosphatidylserine "flipping" (as shown by staining with annexin V staining). The early stages of apoptosis occurred in patches in isolated cells, and it appeared that apoptosing cells began to separate from their neighbors. This work has been reported in abstract form (Reportable Outcomes #1 below). It seemed likely that there would need to be coordinated destruction of these structures one cell at a time, even though the junctions are shared between adjacent cells. We investigated changes in structure of the intercellular junctions that attach adjacent cells to each other.

31EG4 cells exhibited well differentiated tight junctions (as shown by immunofluorescence observations of ZO-1, actin and occludin staining). During the course of these experiments we discovered that damage to the 31EG4 epithelium by simple mechanical abrasion elicited a very pronounced wound healing response that was somehow repressed in the cells that had been stimulated to undergo apoptosis. The wound healing occurred in a very precisely controlled series of events. When monolayers (grown on coverslips or filters) were wounded, transepithelial resistance (TER) dropped by 50-85%, and leading edge cells extended lamellipodia (time lapse DIC microscopy). Confocal fluorescence microscopy was performed on healing monolayers fixed at various times following wounding. Immediately following wounding, cells along the free edges retained their tight junctions (as shown by antibody staining for F-actin, ZO-1 and occludin) for about 10 mins, even though contact with adjacent cells had been disrupted. However, during the course of the next 20 mins, tight junctions disappeared and lamellipodia were formed in the regions of the cells that were no longer in contact with their neighbors. As cells along the free edges continued to migrate and lamellipodia from cells on opposite sides of the wounds touched, ZO-1, occludin and foci of actin re-localized at cell-cell contacts in a characteristic sequence over the course of 60 mins. Perijunctional actin arcs occasionally, but not always, formed in leading edge cells surrounding wounds, indicating that the arcs were not required for cell movement and

membrane polarization in both large and small wounds (with and without lamellipodia). Re-formation of intercellular junctions appeared to occur at specific sites of contact between lamellipodia. These experiments showed that tight junctions were dynamic structures capable of rapid dissolution and reformation during release and then recontact from neighboring mammary epithelial cells. These results will provide useful data relevant to further studies of epithelial and tight junction structure during apoptosis and also for investigations of mammary epithelial cell metastasis following transformation.

An abstract (Reportable Outcomes #2 below) and paper (Reportable Outcomes #3 below) summarizing these results is being written.

3. Measure Ca transport and signaling in the cytosol, ER and mitochondria.

3a. Ca transport and signaling in the cytosol and ER using fluorescence imaging microscopy. We began by determining Ca transport properties of the plasma membrane and internal store (ER) from measurements of [Ca] in the cytosol using fura-2 in control and apoptotic 31EG4 cells. Cells were loaded with the dye, and the response to thapsigargin (inhibitor of the SERCA Ca pump in the ER) was assessed. The magnitude of the initial response to thapsigargin was used as an indirect estimate of Ca release from the ER, and the secondary, sustained response was used as an estimate of Ca entry across the plasma membrane. The thapsigargin response was attenuated by >50% in cells that were undergoing apoptosis, as assessed in the same cells using the SYTO dyes as described above. This indicated that the magnitude of the Ca store in the ER and the entry of Ca across the plasma membrane were both reduced during apoptosis.

A series of experiments characterized the Ca entry pathway across the plasma membrane that also appeared to be inhibited during apoptosis. Measurements using fura-2 showed that the Ca entry pathway was blocked by the Ca channel blocker La with half maximal inhibition occurring at 0.8 μM.

Accompanying the reduction in the apparent size of the ER Ca store, we also observed a localized accumulation of fura-2 indicating a region of high [Ca] in the center of the nucleus which was undergoing the characteristic degradation. A series of experiments was performed using deconvolution microscopy to characterize this process. The general idea was to use the SYTO dye to identify the degrading nucleus and fura-2 to identify regions of high [Ca], which were likely to be associated with the ER. Careful sectioning of the cells showed that regions with high [Ca] had shrunk and become entirely surrounded by the degrading nucleus. It was even possible that these regions had become incorporated into the nucleus. However, the images were not sufficiently distinct to permit unequivocal identification. The apparent close association of the nucleus and the

ER was quite unexpected but may be important for localizing Ca signaling processes during apoptotic degradation of the nucleus. This is a potentially important finding, and we plan to complete these experiments using a confocal microscope that may permit better resolution. This work will be reported at a later time.

3b. Electrophysiological analysis of Ca entry into mammary epithelial cells. Patch clamp experiments were begun to test whether the Ca entry mechanism was through the well known Ca-release-activated Ca channel (CRAC). The idea was to try to correlate results from the fluorescence measurements of cytosolic [Ca] (particularly the La sensitivity of Ca entry) to patch clamp measurements of CRAC activity. Both single channel detached patches and whole cell measurements were performed using Ca-free, Na-containing solutions, conditions that lead to Na entry through CRAC at rates that can be measured using patch clamp methods. It was difficult to obtain reproducible results due to the small currents traversing the CRAC. We spent a great deal of time perfecting methods to obtain patch clamp membrane seals that were tight enough to ensure that leak currents were smaller than CRAC. We reported our findings in an abstract (Reportable Outcomes #4), but we were never confident enough in our CRAC recordings to be able to complete experiments describing changes in Ca entry into mammary epitehlial cells during control and apoptosis.

During the above-mentioned control experiments, a number of different ion channels were identified. These were easier to identify and perform experiments on because they were larger and specific drugs were available to inhibit them. These ion channels included the well known Na (ENaC) and Cl (CFTR) channels that are found in many other secretory epithelia. These ion channels were characterized in some detail to try to determine their potential roles in the ion and fluid transport properties of the mammary epithelium. ENaC was blocked by amiloride and not affected by the presence of Cl, while CFTR was blocked by the well known blocker DPC and activated by elevating cellular [cAMP]. These measurements meshed well with those or our colleague Sheldon Miller, who was performing similar experiments on the same 31EG4 cells in an attempt to determine transepithelial ion and fluid transport properties of the intact 31EG4 epithelium. We collaborated on a study using transepithelial measurements of ion currents and fluid flow along with RT-PCR, western blots and immunofluorescence to show that ENaC and CFTR were both located in the apical membranes of mammary gland cells. 31EG4 MEC monolayers also secreted or absorbed fluid in the resting state, and either amiloride (block ENaC) or cAMP (activate CFTR) increased fluid secretion. We concluded that 31EG4 mammary epithelial cells absorb Na through apical ENaC and secrete Cl through apical CFTR. Equivalent circuit analysis of microelectrode data showed that tight junctions were important in providing counterion movements during both absorption and secretion of NaCl. Thus, mammary cell ENaC, CFTR and also tight junctions were important in controlling the ion and water

composition of milk. These transport processes may also lead to enlargement of the breast cysts that are often observed in postmenopausal women and which are often misdiagnosed as breast tumors. The paper (Reportable Outcomes #4 below) describing these results has been reviewed by the American Journal of Physiology (Cell) and the revised version should be ready to return to the editor very soon.

We have also discovered two K channels in these mammary epithelial cells, an outward and an inward rectifier. One of these is sensitive to the well known K channel blocker Ba while the other is not. These findings are being correlated to experiments being performed by Sheldon Miller's lab to determine which of these K channels is in the apical and which is in the basolateral membrane of the 31EG4 mammary epithelial cells. These channels are likely to be important for regulating membrane potential across the apical and basolateral surfaces of the epithelial cells, and the membrane potential will in turn regulate the transport of Ca, Na and Cl into and out of the cells. We hope to incorporate these results into the revision of the Blaug et al paper to be able to provide a comprensive model for how mammary epithelial cells secrete and absorb fluids.

REPORTABLE OUTCOMES

1. Lee, R. J., and T. E. Machen. Apoptosis induction in cultured mammary epithelial cells. Molecular Biology of the Cell. Nov., 1998. 9(SUPPL.):488A, 1998.

2. Giorgi, G., and T.E. Machen. Occludin and ZO-1 are selectively remodeled at the wound edge of mammary epithelial cells. Molecular Biology of the Cell. 9(SUPPL.):83A, 1998.

3. Giorgi, G., and T.E. Machen. Junctional remodeling during wound healing in mammary epithelium. In preparation.

4. Chandy, G., K. Hybiske, P. Woo, G. L. Firestone and T.E. Machen. Thapsigargin increases Ca^{2+} entry and P_o of a 4-6 pS cation channel in cultured mammary epithelial cells, 31E4. J. Gen. Physiol. 110(1):39A, 1997

5. Blaug, S., K. Hybiske, J. Cohn, G.L. Firestone, T.E. Machen and S.S. Miller. ENaC and CFTR dependent ion and fluid transport in mammary epithelia. American Journal of Physiology (Cell), in review.

Degrees obtained through support of this grant:

Gisele Giorgi, PhD University of California – Berkeley, 1999. Thesis: Wound healing and tight junction formation in mammary epithelial cells

Positions obtained through support of this grant:

Rebecca J. Lee, PhD. Imaging Microscopy Technician at University of New Mexico.

CONCLUSIONS

1. During apoptosis mammary epithelial cells undergo slow changes in structure, including shrinkage of the cells and separation from their neighbors, blebbing of the plasma membrane, condensation and lobing of the nucleus and accumulation of the ER within the lobed structure of the nucleus.

2. Mammary epithelial cells have typical tight junctions between the cells. These junctions are subject to rapid morphological changes in response to mechanical wounds and subsequent healing. ZO-1, actin and occludin are characteristically found at regions where cells form junctions, and following wounding these proteins are removed actively (i.e., by actions of the cells) in regions where adjacent cells no longer touch each other. Tight junctions in the other regions of the cells are maintained during the healing process when cells along the free edges extend pseudopodia and crawl to cover the space between the wound edges. During reformation of the intact monolayer, junctional proteins are rapidly inserted into the membranes in a sequential process that begins in regions of the two cells that first make contact. This is followed by a "zippering up" of the adjacent regions between the cells, with final reformation of the intact monolayer requiring cell division approximately 12-24 hrs later.

3. Ca signaling in control cells is under the control of Ca release from the ER and Ca entry across CRAC-like channels in the plasma membrane that are blocked by La. During apoptosis, Ca release from the ER and Ca entry from outside the cell is reduced by about 50%.

4. Mammary epithelial cells also exhibit Na absorption and Cl secretion, and the well known ion channels ENaC and CFTR are located apically in these cells. These ion channels work in concert with tight junctions to determine the direction and magnitude of fluid flow across the epithelium. These cells also have apical and basolateral K channels that have distinct properties, and these channels are important for maintenance of proper membrane voltage to assure Na and Cl transport through the ENaC and CFTR respectively.

APPENDICES

Copies of # 5 from above list have been included.

ENaC AND CFTR DEPENDENT ION AND FLUID TRANSPORT IN MAMMARY EPITHELIA

Sasha Blaug[1,2], Kevin Hybiske[1], Jonathan Cohn[3], Gary L. Firestone[1], Terry E. Machen[1] and Sheldon S. Miller[1,2]

Department of Molecular and Cell Biology[1] and School of Optometry[2]
University of California at Berkeley
Berkeley, CA 94720-3200

[3]Departments of Medicine and Cell Biology
Duke University Medical Center
Box 3378
Durham, NC 27710-0001

Running title: ENaC, CFTR and shunt resistance in mammary cells

Address for correspondence:

Sheldon S. Miller
360 Minor Hall
University of California at Berkeley
Berkeley, CA 94720-2020
smiller@socrates.berkeley.edu
Tel: 510-642-7769
Fax: 425-952-0627

ABSTRACT

Mammary epithelial 31EG4 cells (MEC) were grown as monolayers on filters to analyze the apical membrane mechanisms that help mediate ion and fluid transport across the epithelium. RT-PCR showed the presence of CFTR and ENaC message and immunomicroscopy showed apical membrane staining for both proteins. CFTR was also localized to the apical membrane of native human mammary duct epithelium. In control conditions, the mean values of transepithelial potential (TEP, apical side negative) and resistance (R_T), are -5.9 mV and 829 $\Omega \cdot cm^2$, respectively. The apical membrane potential (V_A) is - 40.7 mV and the mean ratio of apical to basolateral membrane resistance (R_A/R_B) is 2.8. Apical amiloride hyperpolarized V_A by 19.7 mV and tripled R_A/R_B. A cAMP-elevating cocktail depolarized V_A by 17.6 mV, decreased R_A/R_B by 60%, and increased short-circuit current (I_{SC}) by 6 $\mu A/cm^2$ and decreased R_T by 155 $\Omega \cdot cm^2$, and largely eliminated responses to amiloride. Whole cell patch clamp measurements demonstrated amiloride-inhibited Na currents (linear I-V) and forskolin-stimulated Cl currents (linear I-V). A capacitance probe method showed that in the control state, MEC monolayers either absorbed or secreted fluid (2 - 4 $\mu l \cdot cm^{-2} \cdot hr^{-1}$). Fluid secretion was stimulated either by activating CFTR (cAMP) or blocking ENaC (amiloride). These data plus equivalent circuit analysis showed that: (1) fluid absorption across MEC is mediated by Na transport via apical membrane ENaC and fluid secretion is mediated, in part, by Cl transport via apical CFTR; (2) in both cases, appropriate counterions move through tight junctions to maintain electroneutrality; (3) activation of CFTR appears to inactivate ENaC. Interactions among CFTR, ENaC, and tight junctions allow MEC to either absorb or secrete fluid and *in situ* may help control luminal [Na] and [Cl].

Key Words: amiloride, DPC, milk secretion, patch clamp, microelectrodes, electrophysiology, cystic fibrosis, tight junctions, leaky and tight epithelia

INTRODUCTION

The mammary gland is a branched, convoluted tubular organ with acinar cells that secrete macromolecules (milk proteins, lactose, fats), salts (including Na, K, Ca, Cl and phosphate) and water. Human milk contains approximately 200 mM lactose, 7 mM Na, 13 mM K, 8 mM Ca, 12 mM Cl and is mildly acidic (pH 6.8) (34). The initial secretion of milk by the acinar cells probably occurs as an isotonic fluid, largely driven by the production and then secretion of lactose and osmotically obliged fluid. The duct cells likely modify this fluid as it moves along the duct and passes out to the nipple. It is possible that the relatively low ionic content of milk is either generated or maintained by the reabsorptive properties of acinar and duct cells, but the specific ion channels and other transporters involved have not been described.

Abnormal fluid accumulation in the breast is common in premenopausal women (5, 6, 21, 30). As part of a project to determine how mammary cysts accumulate fluid, we began a study of the ion transport properties of the mammary epithelial cell line 31EG4. This untransformed mouse cell line appears to have properties of both acinar and ductal mammary epithelia cells (39, 42, 48). Previous experiments on primary cultures of mouse mammary epithelial cells, which are a mixture of duct and acinar cells (4), showed that Na is actively absorbed, that this absorption is stimulated by the lactogenic hormone prolactin, and that absorption is inhibited by apical amiloride, the well known blocker of the epithelial Na channel (ENaC; (19)). 31EG4 cells form polarized monolayers with tight junctions that are regulated in their "tightness" by the glucocorticoid dexamethasone, which can stop growth and induce differentiation (48). This process includes an increase in transepithelial resistance (R_T) from 100 - 300 $\Omega \cdot cm^2$ to > 700 - 1000 $\Omega \cdot cm^2$, and the appearance of tight junctional proteins ZO-1 and more "organized" filamentous actin. It is thought that this regulation of tight junctions recapitulates the transformation of mammary cells from a leaky to a tight epithelium characteristic of the lactating gland that must maintain a large transepithelial (blood to milk) concentration gradient for ions and macromolecules (29, 35). Coincident with the increase in R_T,

31EG4 cells also express Na/H exchange and Na/HCO_3 cotransport activity in the basolateral, but not the apical, membrane (41).

The goal of the present work was to determine whether the epithelial Cl and Na channels (cystic fibrosis transmembrane conductance regulator, CFTR, and ENaC, respectively) contribute to the ion and fluid transport properties of the mammary epithelial cell line 31EG4. We reasoned that since mammary and sweat glands are of similar embryological origin and have several characteristics in common, and sweat duct cells express high levels of both these ion channels to allow reabsorption of salt from the fluid that flows down the duct (38), 31EG4 cells might also express these ion channels. We used RT-PCR to identify the message, western blot and immunomicroscopy to identify the proteins. In experiments utilizing transepithelial, microelectrode and patch clamp techniques, amiloride-inhibitable changes in voltage and resistance were used to localize ENaC to the apical membrane and stimulation with cAMP and inhibition by DPC (diphenylamine-2-carboxylate) showed that CFTR is localized to the apical membrane. The roles of ENaC and CFTR in fluid absorption and secretion were determined by measuring amiloride- and cAMP - induced changes in fluid transport (capacitance probe method).

MATERIALS AND METHODS

Cell culture

31EG4 cells were grown and cultured in DMEM/F12 media containing 5% fetal bovine serum (FBS), 5 μg/ml insulin and 5 μg/ml gentamicin sulfate. Upon reaching confluency, these cells, passage six to ten, were plated onto Transwell filters (Costar) at a density of 10^5 cells/well. They were grown in DMEM/F12 containing glutamine, 2% FBS, and insulin and gentamicin as described above. When the cells became confluent on the filters, 1 μM dexamethasone was added to stop growth and induce differentiation, including formation of tight junctions (48) and polarization of ion transport pathways to the apical and basolateral membranes (41). Transepithelial resistance (R_T) and voltage (TEP) were estimated using an EVOM (Epithelial Voltammeter, World Precision Instruments, New Haven CT). The experiments were all carried out between days six and nine days following the addition of dexamethasone with no discernable differences in mean TEP or R_T.

RT-PCR

Total RNA was extracted from 3lEG4 cells using the RNAzol B method (Teltest) per manufacturer's instructions. First strand cDNA synthesis was carried out by using 0.5 pg of total RNA, 20 pM oligo-dt primers, 0.5 mM dNTP mix, and 200 units of MMLV reverse transcriptase in a final volume of 20 ml of 50 mM Tris-HCl (pH 8.3), 75 mM KCl, and 3 mM $MgCl_2$. The RNA and oligo-dts were annealed by first mixing the two items, heating to 70°C for 2 min and then cooling on ice followed by the addition of the remaining reaction components. The mixture was incubated at 42°C for 1 hr for first strand synthesis and then heated to 94°C for 4 min to stop the reaction. The mixture was then diluted 1:5 with sterile distilled water. A control reaction containing no reverse transcriptase was included for each tissue reverse transcriptase reaction to assure that no genomic DNA was being amplified (data not shown).

PCR was carried out using oligonucleotide primers (sense gtgattggagctatagcagttgtcg; anti-sense cccacatctggagcccacagc) designed to cover a 463 base pair region of CFTR and a 596 base pair region of ENaC (sense tgcaactaccggaacttcacg; anti-sense gtactgggtgtcattgcagg). The primers (0.5 mM final concentration) were added to a 1 ml aliquot of the first strand synthesis mixture with the following: 0.2 mM dNTPs (each), 1.25 units of Thermus aquaticus polymerase, PCR buffer with Mg (Boehringer Mannheim) and water to bring to a total volume of 50 µl. The reaction was then overlaid with 2 drops of mineral oil (Sigma). The mixture was then incubated in a thermal cycler (Stratagene) with the following amplification profile: 1 cycle at 94°C for 4 min, 37 cycles at 94°C for 1 min, 55°C for 1 min, 72°C for 1 min, and 1 cycle of 72°C for 10 min. The PCR product was run on a 1.5% agarose gel. This product was excised from the gel with a razor and then purified and sequenced by the U.C. Berkeley Sequencing Center.

Westerns

31EG4 cells were cultured to confluence on filters as described above. Proteins were isolated by placing the cells into 100 µl of protein isolation buffer containing (in mM) 65 NaCl, 2 MgCl2, 1 EDTA, 5 Tris-acetate, pH 7.4, as well as the following protease inhibitors (µg/ml): 2 aprotinin, 2 leupeptin, 1 pepstatin A, 2 antipan, 100 PMSF, 50 TLCK, and 100TPCK. The cells were homogenized by sonicating (Branson, Danbury, CT) on ice for 60 seconds. Protein concentration was determined using BCA Protein assay kit (Pierce, Rockford, IL). To separate protein from membranes, the sample was incubated for 4 hrs at room temperature in 4 % digitonin (w/v) in 0.2 M sodium phosphate buffer, pH 8.6. Electrophoresis of the samples was carried out using Bio-Rad Mini Protein ready gels (7.5% TRIS-HCl) and the Bio Rad Mini-Protean cell (Bio-Rad, Hercules, CA). The running buffer contained 25 mM TRIS, 200 mM glycine and 0.1% SDS. Electroblotting of the proteins onto PVDF membranes was carried out in a BioRad Mini-Trans-Blot cell at 4°C. The transfer buffer contained 25 mM TRIS and 200mM glycine, pH 8.2-8.5. The blotted PVDF membranes were then blocked in 2% casein (in 0.1% (v/v) Tween-20 in PBS) for 1 hr at room temperature (RT) and then incubated with 1:1000

dilution of primary anti-CFTR antibody overnight at 4°C (this antibody, pAbECL1-19, peptides corresponding to amino acids 103-109,109-114,114-119 of CFTR was a generous gift from Genzyme). Similar procedures were used with a primary anti-ENaC antibody (β subunit, a generous gift from Pascal Barbry). The membranes were rinsed three times (5 mins each) with blotto (5% nonfat dried milk and 0.1% Tween-20, in PBS). Next the membrane was incubated in 1:5000 dilution of horse radish peroxidase-conjugated anti-rabbit secondary antibody (Sigma, St. Louis, MO) for 1 hour at room temperature followed by three times (5 mins each) with blotto then 5 mins with PBS. The labeled membranes were developed by the enhanced chemiluminescence method (Renaissance, New England Nuclear, NEL-10).

Immunohistochemistry

31EG4 cells were grown to confluency on transwell filters, and the monolayer and filter membranes were punched out, rinsed in PBS for one minute at RT, and then fixed in 4% formaldehyde-PBS for 30 minutes. The sample was then rinsed three times, over the course of 10 min, with PBS at room temperature and placed in 30% sucrose-PBS solution to equilibrate overnight at 4 °C. Next the samples were embedded in Tissue-Tek O.C.T. compound (Tissue-Tek, Torrance, CA) and incubated at -20°C for at least 1 hr. The samples were then sectioned in 10-20 μm slices using a cryostat (Leica), placed on super-frost glass slides (Fisher Scientific), and left overnight to dry at RT. Sections were rinsed for five mins in PBS and incubated in 10% BSA-PBS solution for 2 hrs at RT. The slides were then incubated overnight at 4°C in 1:100 (PBS/BSA) dilutions of either polyclonal anti-CFTR (Genzyme) or anti-ENaC (β subunit: a gift from Pascal Barbry). The sections were rinsed three times (10min each time) in PBS at (RT) and then incubated in 1:2000 dilution of FITC-labeled secondary antibodies for one hour at RT. The sections were finally rinsed three times (10 min each time) in PBS and mounted on coverslips using Prolong mounting solution (Molecular Probes, Eugene, OR). Images were obtained using a Zeiss Axiophot microscope with a 63X objective.

Immunomicroscopy to identify CFTR in intact mammary gland was also performed on cryosections (4 μm) of promptly frozen normal human surgical specimens using an affinity-purified rabbit antibody (a1468, to a synthetic peptide corresponding to amino acids 1468-1480 of CFTR (11, 31)) at a dilution of 1:200. The specificity of a1468 as a reagent for detecting endogenously expressed CFTR in human colonocytes has been verified in a variety of tissues by immunoblot, immunoprecipitation and immunostaining (11-13, 18, 31). Sections were incubated first with a1468 and then with a monoclonal antibody to cytokeratin 19 (ICN Biomedical, Inc., Costa Mesa, CA). Sections were then washed and incubated with TRITC- and FITC-conjugated goat F(ab')2 fragments (Tago Inc., Burlingame, CA). Controls for immunostaining-included sections stained without primary antibody or with normal rabbit serum.

Fluid transport

Transepithelial fluid flows (J_V) were measured using the capacitance probe technique (22, 24). A monolayer on a filter (0.5 cm^2 exposed area) was mounted between two water-impermeable Kel F half-chambers. JV was determined using a very sensitive oscillator circuit (Acumeasure 1000, Mechanical Technology, Inc., Lantham, NY) connected to two probes, one on either side of the tissue, which measure the capacitance between the probe tips and the fluid meniscuses connected to each half-chamber. Ion-linked fluid is driven across the tissue from its apical to basolateral surfaces, or vice versa. Fluid movement across the epithelium is recorded by the changes in probe output voltage. Ports in the bottom of the half-chambers allow for solution and chemical composition changes on either side of the tissue. The capacitance probe in each half chamber was calibrated by injecting 1 μl volumes of fluid and measuring the probe output in mV (737 mV/μl). This technique has a resolution of ~1 nl/min, corresponding to a fluid transport rate approximately 1/10th the average baseline fluid transport rate seen in the present experiments. Voltage-sensing and current-passing bridges built into each half chamber permit continuous monitoring of transepithelial potential (TEP) and resistance (R_T), the latter calculated from the voltage deflections in response to transepithelial current pulses of known

magnitude. The control Ringer for measurements of J_V, TEP, R_T contained (in mM): 113.5 NaCl, 5 KCl, 26 $NaHC0_3$,1.8 $CaCl_2$, 0.8 $MgS0_4$, 1.0 NaH2P0_4, 5.5 glucose, pH 7.4. In some experiments a cAMP cocktail was added to the control Ringer: 500 M IBMX, 100 μM 8-(4-chlorophenylthio) adenosine 3';5'-cyclic monophosphate (CPT-cAMP), 12 μM forskolin. In other experiments, the following inhibitors were tested: 10-50 μM amiloride (to block ENaC), 0.5 - 1.0 mM DPC (to block CFTR) and 50 μM NPPB (to block CFTR).

Patch clamp electrophysiology

Cells were plated on glass coverslips at low density. Patch pipettes were pulled from glass (WPI, Sarasota, FL) on a microelectrode puller (Narishige, Ltd, Tokyo, Japan) and fire-polished on a microforge (Narishige) to a resistance of 2 - 10 MΩ when filled with intracellular solution (see below). Seal resistances were typically 10 GΩ. Data were recorded in the voltage-clamp mode with an amplifier (Axopatch-1D, Axon Instruments, Foster City, CA) connected to a personal computer with an A/D board. Voltage sweeps and currents were recorded using Clampex acquisition software (Axon Instruments). Leak subtraction was not performed on any of the data. Solution changes were made *via* a 7-node perfusion chamber. Bath chamber was maintained at 37°C using a battery-operated resistive element mounted on the bottom of the chamber and controlled by a battery operated feedback circuit.

To identify CFTR, whole cell patch pipettes were filled with intracellular solution containing (in mM): 121.5 NMDGgluconate, 13.5 NMDGCl, 1.8 ATP, 0.09 GTP, 9 Hepes and 9 glucose. Extracellular solution contained (in mM): 141 NaCl, 4 KCl, 1 KH_2PO_4, 1 $MgSO_4$, 1 $CaCl_2$, 10 Hepes and 10 glucose, with either 10 μM forskolin or 2 mM DPC added. Voltage sweeps were run from -80 mV to 100 mV, with data sampled at a frequency of 10 kHz.

Whole cell experiments were also performed in an attempt to identify ENaC in single 31EG4 cells. Cells were plated at low density and then treated with 1μM dexamethasone for roughly 24 hrs prior to the experiment to increase cellular differentiation. Pipette solution for these experiments contained (in mM): 121.5 NMDGgluconate, 2.7 NMDGCl, 0.9 $CaCl_2$, 0.9

MgCl2, 9 Hepes, 4.5 glucose, 2.25 ATP, 0.09 GTP and 9.9 EGTA. Two different extracellular solutions were employed for these experiments. Extracellular Na gluconate solution contained (in mM): 145 Na gluconate, 7 NaCl, 1 $CaCl_2$, 1 $MgCl_2$, 10 Hepes and 5 glucose. Extracellular NaCl solution contained (in mM): 150 NaCl, 1 $CaCl_2$, 1 $MgCl_2$, 10 Hepes and 5 glucose. Voltage sweeps were run from -80 mV to 100 mV, with data sampled at a frequency of 10kHz. Conductances values were obtained by measuring the slopes of the I-V curves around 20 mV.

Transepithelial and microelectrode electrophysiology

The recording setup and perfusion system has been previously described (36). Transwells with confluent 31EG4 monolayers and $R_T > 300\ \Omega \cdot cm^2$ were used for the electrophysiology measurements. The monolayers on filters were mounted on a nylon mesh support and clamped into a modified Ussing chamber. R_T and the ratio of the apical to basolateral membrane resistance (*a*-value) were obtained by passing 4 μA current pulses across the tissue and measuring the resultant changes in TEP, V_A, and V_B (see below). Current pulses were bipolar, with a period of 3s applied at various time intervals. R_T is the resulting change in TEP divided by 2 μA, and *a* is the ratio of voltage change in V_A divided by the change in V_B ($a = \Delta V_A/\Delta V_B$). The current-induced voltage deflections were digitally subtracted from the records for clarity. Short circuit current (I_{SC}) measurements were performed using similar chambers and electrophysiological apparatus, with TEP clamped to zero and using solution and resistance compensation. 5 mV pulses were often utilized to measure R_T in these experiments. The control Ringer (in mM) for measurements of TEP, R_T and I_{SC} are identical to those used for the fluid transport measurements described above.

Calculating membrane and shunt resistances and equivalent electromotive forces

The intracellular measurements were analyzed using an equivalent circuit model (see Fig. 1) that has been previously described (26, 32). We used the microelectrode data to calculate resistances (R, $\Omega \cdot cm^2$) and equivalent electromotive forces (E, mV) for the apical and basolateral

membranes and shunt for 31EG4 cells. The general approach (26) was to measure TEP as well as voltages across the apical (V_A) and basolateral (V_B) membranes and a-values ($a = \Delta V_A/\Delta V_B = R_A/R_B$) in control conditions and then during treatment with amiloride. This allowed us to calculate shunt resistance (R_S). It was assumed that amiloride only altered E_A and R_A. Calculation of equivalent circuit parameters was based on the following steady state considerations:

$$(1)\ V_A = E_A + iR_A \quad \text{and} \quad V_B = E_B - iR_B$$

where *i* is the loop current generated by the difference in V_A and V_B and E_A and E_B are the apical and basolateral membrane potentials that would be recorded if R_S were infinite. By definition:

$$(2)\ TEP = V_B - V_A \text{ and } i = TEP/R_S$$

R_T is given by:

$$(3)\ R_T = [(R_A + R_B)R_S]/[R_A + R_B + R_S] \text{ and } a = R_A/R_B$$

Combining (1) and (2) gives:

$$(4)\ V_A = E_A + TEP(R_A/R_S)$$

Similarly,

$$(5)\ V_B = E_B - TEP(R_B/R_S)$$

Using eqn. 3 before and after amiloride (denoted with *) gives:

$$(6)\ R_S = [R_T R_T^*(a^* - a)]/[R_T(1 + a^*) - R_T^*(1 + a)]$$

Using eqns (4) - (6) and the data collected before and shortly after amiloride we calculated R_S, then R_A, R_B, E_A and E_B for control and amiloride-treated conditions. This calculation assumes that amiloride affects only the apical membrane, while R_S and R_B remain constant.

Data are presented as mean ±SE, unless otherwise specified. Student's unpaired t-test is used to compare groups and $P < 0.05$ is considered statistically significant.

RESULTS

PCR, westerns and immunocytochemistry

PCR and western blot analysis were performed on 31EG4 cells grown to confluence in the presence of dexamethasone to increase differentiation of the cells. The PCR experiments summarized in Fig. 2 showed that mRNA for both ENaC and CFTR was present in 31EG4 cells. In Fig. 3, western blots with bands at 170 kDa (CFTR) and 85 kDa (ENaC β subunit) indicated that both proteins were being made.

Immunomicroscopy was performed on 31EG4 cells grown to confluence on filters. As shown in Figs 4A and B, both ENaC and CFTR appeared to be expressed in the apical portions of the 31EG4 cells. CFTR immunoreactivity was also detected in intact human mammary glands by indirect immunofluorescence (Fig. 5). The predominant site of staining was the apical domain of the epithelial cells lining the ducts of the mammary gland. Cytokeratin staining identified duct cells and demonstrated tissue architecture for orientation.

Transepithelial and patch clamp electrophysiology

31EG4 monolayers were mounted in Ussing chambers and then treated with amiloride (to block ENaC) followed by forskolin (to stimulate cAMP production and active PKA) and DPC (to block CFTR). As shown in Fig. 6, 10 μM amiloride in the apical solution decreased I_{SC}, though not to zero, indicating that there was some residual anion secretion or cation absorption. The identity of this ionic current has not been identified. Instead we have concentrated on determining the potential contribution of ENaC and CFTR to the ion transport properties of 31EG4 cells. In the presence of apical amiloride, forskolin (10 μM) increased I_{SC}, and subsequent addition of apical DPC (500 μM) decreased I_{SC}. In five experiments, amiloride decreased I_{SC} by 2.5 ± 0.7 μA/cm^2 (mean ± SE); in the presence of amiloride, forskolin increased I_{SC} by 7.8 ± 1.4 μA/cm^2 and subsequent addition of DPC decreased I_{SC} to by 5.5 ± 0.8 μA/cm^2.

Whole cell patch clamp measurements were also performed on 31EG4 cells. As shown in Fig. 7A, forskolin increased cellular conductance from 1.7 nS to 34 nS and shifted the reversal potential from about -20 mV to -25 mV. DPC reversed the forskolin-induced changes by bringing the reversal potential and the conductance back to their resting, baseline levels. Fig. 7B summarizes the effects of forskolin and DPC on 31EG4 cell conductance.

Amiloride-sensitive currents were also identified in whole cell patch clamp experiments. These currents were quite small in the resting state (Fig. 8A), so the inhibitory effects of amiloride were difficult to identify in every cell. Fig. 8A shows an experiment in which the cells were incubated in a NaCl-containing Ringer solution; the I-V curve showed small, linear currents (mean whole cell conductance = 0.6 nS, reversal potential = -15 mV). Conductance was inhibited by amiloride to 0.3 nS, and the reversal potential shifted in the negative direction to -22 mV, consistent with inhibition of ENaC. Two other experiments were also performed on cells in which the bathing solution was Na gluconate Ringer's (to eliminate contribution of Cl currents), and amiloride had similar effects on cell currents and conductances, although the absolute conductances were, for some unexplained reason, significantly higher. Fi. 8B summarizes the results from two experiments in which the cells were incubated in a NaCl - containing Ringer (filled circles) and two other experiments in which the cells were bathed in Na gluconate Ringer (open circles).

Intracellular recordings, calculated EMF's and cell membrane resistances

Fig. 9 illustrates a typical intracellular microelectrode recording with resting, unstimulated levels of V_A, V_B, TEP, R_T, and R_A/R_B. When a cocktail of forskolin, CPT-cAMP and IBMX was added to the apical bath (black bar), there was a rapid and reversible increase in TEP since V_A depolarized more than V_B; concomitantly, R_T dropped, and R_A/R_B decreased from 3.5 to 2. All these responses are consistent with a conductance increase of an apical membrane channel whose equilibrium potential is depolarized with respect to V_A.

As summarized in Table 1A, the mean resting R_T and TEP are 829 $\Omega \cdot cm^2$ and -5.9 mV, respectively. The TEP is apical side negative since V_B is more hyperpolarized than V_A. In addition, the mean $R_A/R_B \approx 3$ indicates that the apical membrane has a three-fold greater resting resistance than the basolateral membrane. Table 1B summarizes the cAMP-induced changes in membrane voltages and resistance, which are all consistent with an increase in apical membrane conductance. Using the summary data in Table 1A,B the calculated (Ohm's law) equivalent short circuit current of the resting monolayer increased from 7.1 $\mu A/cm^2$ to 12.1 $\mu A/cm^2$ following treatment with the cAMP-raising cocktail, similar to the forskolin-induced increase in I_{SC} measured in the experiment in Fig. 6. The results illustrated in Figs 6 and 9 and summarized in Table 1B are consistent with the hypothesis that cAMP activates apical membrane CFTR and increases Cl transport from the basolateral to the apical surface at a rate of ≈ 5 $\mu A/cm^2$.

Since the CFTR-blocker DPC appeared to block the forskolin-induced increases in I_{SC} (Fig. 6), it was expected that the cAMP-induced changes in cellular electrophysiology would also be blocked by NPPB, another fairly specific CFTR-blocker (25, 40). In the presence of apical NPPB (see Fig. 10), the cAMP cocktail had relatively little or even opposite effects on R_T, R_A/R_B, TEP, V_A and V_B (compare to following control or Fig. 10). For example, the slow decrease in TEP shows that V_B depolarized faster than V_A in the presence of NPPB, opposite to what is seen for the cAMP-induced changes in TEP and membrane potential. Practically identical NPPB-induced responses were observed in four experiments. In sum, elevating cell cAMP depolarized V_A and V_B, decreased R_A/R_B and R_T and increased TEP (Table 1B). These changes and their blockade by apical NPPB (or DPC, in Fig. 6) are all consistent with the presence of CFTR at the apical membrane.

Intracellular recordings were also used to measure the effects of amiloride on membrane voltages and resistances. Results from a typical microelectrode experiment are shown in Fig. 11 where apical amiloride (20 μM) decreased TEP and increased R_T. R_A/R_B increased by more than a factor of six, and V_A hyperpolarized by 24 mV. All the electrophysiological changes were reversed when amiloride was removed from the apical bath. Similar amiloride-induced changes

were obtained in 16 experiments and are summarized in Table 1B. These results indicate that amiloride blocked Na entry through apical ENaC.

Addition of 20 μM amiloride to the basolateral solution caused small and equal depolarizations (<5 mV) in V_A and V_B with no change in TEP, a 30% drop in R_A/R_B and a 5% increase in R_T (n = 3; not shown). These small alterations in membrane voltage and resistance may have been due to the effect of amiloride on the basolateral Na/H exchanger (41) and secondary changes in cellular pH.

The data summarized in Table 1 were used as described in the Methods to calculate resistances and EMF's for the apical and basolateral membranes and shunt for 31EG4 cells in control and during amiloride. The results of these calculations are summarized in Table 1C. The assumption (Methods) that amiloride had no affect on R_S or R_B was tested by allowing either R_S or R_B to change up to ± 20%, following amiloride. In both cases, all of the calculated parameters were within 0.5 SD of the mean values shown in Table 1, indicating that within the error of these experiments the effects of amiloride were restricted to the apical membrane.

Comparison of amiloride effects under control and cAMP or ATP-treated conditions

Previous experiments have shown increased Na and fluid absorption in cystic fibrosis tissues (7, 20, 24), and heterologous expression of CFTR is known to decrease the activity of ENaC in both frog oocytes (27) and MDCK cells (43, 44). However, it has also been shown that ENaC activity is much reduced in freshly isolated CF sweat ducts that lack functional CFTR (38). Since 31EG4 cells express both CFTR and ENaC, we tested whether cAMP treatment could alter ENaC activity. A typical experiment is shown in Figure 12A. In the first part of the experiment, amiloride (20 μM) hyperpolarized V_A by 20 mV and increased baseline R_A/R_B by a factor of ten, from 0.25 to 2.5; in addition, R_T increased and TEP decreased. Subsequent addition of the cAMP cocktail, in the continued presence of amiloride, depolarized V_A by ≈ 24 mV and decreased R_A/R_B to its baseline level in control Ringer. Cyclic AMP addition also decreased R_T and increased TEP. Similar results were obtained in two other experiments (not shown). The

voltage changes were somewhat larger than those exhibited in the absence of amiloride, probably because amiloride increased the driving force for Cl exit across the apical membrane. These results show that the blockade of ENaC activity with amiloride does not appreciably alter the cAMP-induced changes in membrane voltage and resistance.

In contrast, the data in Figure 12B show that apical amiloride caused significantly smaller electrophysiological changes in the presence of cAMP stimulation: V_A and V_B hyperpolarized by only 5 mV, and R_A/R_B, R_T, and TEP hardly changed in the presence of cAMP (Table 1B). Equivalent circuit calculations of membrane resistances and voltages were also performed on the subset of microelectrode experiments in which amiloride was added to monolayers that had been treated with cAMP. Results from these calculations have been summarized in Table 2B. Compared to control conditions (Table 1C), cAMP caused R_A to decrease by more than a factor of ten. In the presence of cAMP, amiloride had essentially no effect on R_A, suggesting that ENaC activity is significantly reduced when CFTR is activated by cAMP.

The putative reduction in ENaC activity might, however, also be secondary to cAMP-induced changes in membrane voltage or resistance. This possibility was tested by activating another set of apical Cl channels to see if they also reduced the effects of amiloride. We have found that the apical membrane of 31EG4 cells contains P2Y receptors that when activated by ATP elevate cell calcium (SB and SM, in preparation) and produce membrane voltage and resistance changes very similar to those produced by elevating cell cAMP: in seven experiments, apical ATP (50 μM) depolarized V_A by ≈17 mV, from –43.9 ± 1.7 mV to –26.9 ± 1.1 mV; R_A/R_B decreased from 3.5 ± 0.2 to 1.8 ± 0.3 and R_T decreased by 109 Ω·cm^2, from 518 ± 39 Ω·cm^2 to 409 ± 20 Ω·cm^2 (mean ± SEM), changes not significantly different from those produced by cAMP (Table 1B). If the reduction in ENaC activity were entirely dependent on cAMP-induced changes in membrane voltage or resistance, then activation of Ca^{2+}-activated Cl channels by ATP should also inhibit the amiloride–induced changes in TEP and R_T.

The experiment summarized in Fig. 12C tested this notion by comparing, in the same monolayer, the amiloride responses, first in the presence of cAMP (top panel) and then in the

presence of ATP (bottom panel). Identical results were obtained independent of order. Apical amiloride characteristically decreased TEP and increased R_T, and these responses were reversible. In the presence of cAMP (which increased TEP and decreased R_T) amiloride had no significant effect on TEP or R_T. The cAMP cocktail and amiloride were removed, and the monolayer was returned to control Ringers for 30 minutes. The bottom panel (same monolayer) shows that the addition of ATP to the apical bath had effects on TEP and R_T nearly identical to those produced by cAMP. In the presence of ATP, amiloride decreased TEP and increased R_T by amounts that were very similar to control, untreated monolayers. These results are summarized in Table 3. The amiloride-induced changes in TEP and R_T are significantly reduced in the presence of cAMP, but not in the presence of ATP, indicating that the apparent cAMP-induced reduction in ENaC activity is not caused by changes in membrane voltage or resistance per se.

Fluid transport

Rates of transepithelial fluid movement along with TEP and R_T were measured under baseline, control conditions in 31EG4 monolayers grown on filters and then following the addition of either a cAMP-stimulating cocktail or amiloride to the apical bath. Figure 13 summarizes the data from a cAMP experiment. The baseline J_V was $\approx$ 3.5 $\mu l \cdot cm^{-2} \cdot hr^{-1}$, in the absorption direction. Addition of cAMP cocktail reversibly altered TEP and R_T, as in the electrophysiology experiments. Consistent with increased Cl secretion, cAMP reversed the direction of steady-state fluid flow from absorption to secretion ($\approx$ -2.5 $\mu l \cdot cm^{-2} \cdot hr^{-1}$); this J_V response was partially reversible.

In control Ringer, the direction and magnitude of fluid transport was variable, independent of time in culture (six to nine days).[1] In 17 cultures (summarized in Fig. 14), nine exhibited a baseline absorption (range: 0.5 to 7.6 $\mu l \cdot cm^{-2} \cdot hr^{-1}$) and eight exhibited a baseline secretion (range: 0.75 to -5 $\mu l \cdot cm^{-2} \cdot hr^{-1}$. Cyclic AMP always caused fluid secretion[2], which ranged from -1 to -8 $\mu l \cdot cm^{-2} \cdot hr^{-1}$. The cAMP-induced changes in TEP and R_T were very similar for both fluid absorbing and secreting tissues and very similar to the electrophysiological results

summarized in Table 1B. In six other monolayers, two absorbing and four secreting (Fig. 14, closed circles), apical amiloride increased the mean secretory rate to -6.7 ± 4.8 $\mu l \cdot cm^{-2} \cdot hr^{-1}$ (mean $\pm$ SD).

In Figure 15 we have plotted the magnitude ($|\Delta J_V|$) of the cAMP-induced fluid secretory response (left-hand axis) as a function of steady-state J_V. $|\Delta J_V|$ was largest for those monolayers that absorbed fluid in the baseline condition (before addition of cAMP) and lowest for those that secreted fluid. Figure 15 also shows that for monolayers in the baseline condition (no amiloride or cAMP), R_T (right-hand axis) was highest in monolayers that absorbed fluid and lowest in monolayers that secreted fluid in the baseline condition.

DISCUSSION

CFTR, ENaC, ion transport, tight junctions, and mammary gland physiology

The normal (i.e., non-transformed) mammary epithelial cell line 31EG4 expresses CFTR and ENaC in the apical membranes. Messages for both CFTR and ENaC were identified, and western blots showed that proteins with the expected molecular sizes were present. Immunomicroscopy of the cultures and intact human mammary tissue (Figs. 4 and 5) indicated that both channels are located either in or very close to the apical membrane. Although the immunomicroscopy could not determine the precise membrane locations of CFTR and ENaC, electrophysiology indicated that these channels were active in the apical membranes of the cells.

In the short circuited condition, or using open circuit TEP and R_T data to calculate equivalent short circuit current, 31EG4 cells exhibited currents of 2 - 7 $\mu A/cm^2$ that were blocked by apical, but not basolateral, amiloride. Whole cell patch clamp measurements also demonstrated amiloride-inhibited currents and conductance and linear I-V curves expected for ENaC. Microelectrode experiments showed that amiloride hyperpolarized E_A and caused large increases in R_A, consistent with blocking apical ENaC. Cyclic AMP depolarized E_A and reduced R_A by more than a factor of 10 (compare Table 1C and Table 2B) and also increased basolateral-

to-apical anion current (likely Cl or HCO_3) by 5 $\mu A/cm^2$; these changes were inhibited by apical DPC or NPPB. Patch clamp experiments also showed forskolin-stimulated, DPC-inhibitable currents and conductance, and linear I-V curves. Cyclic AMP treatment may also have altered the voltage or conductance properties of the basolateral membrane (46), but clearly a major effect of cAMP stimulation was to activate apical CFTR. 31EG4 cells also express apical membrane ATP-activated Cl channels and apical and basolateral K channels (unpublished) that were less completely characterized. These channels may contribute to the negative values of E_A and E_B and could also be important for ion and fluid secretion (and absorption) that occur in both baseline (control) and cAMP-stimulated conditions.

Our calculations that R_S (1000 - 1400 $\Omega \cdot cm^2$) is smaller than total cellular resistance ($R_{cell} = R_A + R_B$ = 2100 -2500 $\Omega \cdot cm^2$) indicate that although R_S (Table 1) is large compared to many tissues with "leaky" tight junctions (R_S < 100 - 200 $\Omega \cdot cm^2$; see (14)), it is apparently still a major pathway for current flow. The low value of R_S compared to R_{cell} also helps keep the TEP in 31EG4 cells relatively small, -6 mV, similar to the situation in leaky epithelia (32). As will be discussed below, this tight junctional permeability also contributes to the ability of 31EG4 cells, a clonally derived cell line (39, 42, 48) with roughly equal distributions of ENaC and CFTR in all the cells of the monolayer (Figs 4 and 5), to both secrete and absorb fluid (Fig. 14 and Footnote 1). It will be interesting to determine whether acinar and ductal cells *in situ* retain this capability or if the present results represent a culture-to-culture variation in the ratio of secretory (acinar?) to absorptive (ductal?) epithelial cells.

The present demonstration of functional ENaC in the apical membrane of 31EG4 cells is consistent with previous experiments showing amiloride-sensitive Na absorption across short circuited primary cultures of both midpregnant and lactating mammary gland cells (3). Similarly, localization of CFTR to the lumenal membrane of 31EG4 cells is consistent with the presence of apical CFTR in native human mammary duct cells (Fig. 5). Our results therefore indicate that ENaC and CFTR of mammary duct cells may be involved in generating or maintaining the characteristic Na and Cl concentrations of milk (34).

ENaC and CFTR may also be involved in the abnormal generation and accumulation of breast fluid (so called cystic disease of the breast) that occurs in seven to ten percent of women in Western countries, mainly in the premenopausal decade. There is now strong evidence to indicate that these women are at a 2-4-fold higher risk of later developing breast cancer (5, 8, 10, 16, 30). Although the chemical compositions of these fluid-filled cysts are quite complicated (1, 9), there appears to be a distinct pattern of Na and Cl concentrations (17, 33) that could reflect alterations in luminal CFTR and ENaC activity. Clinically, it has been shown that tamoxifen reduces the number and size of such cysts (28). Since tamoxifen can block Cl channels (15, 47), it may be exerting its therapeutic effect by decreasing fluid secretion.

Critical role of tight junctions in ion and fluid transport

The present data using 31EG4 monolayers and evidence from other epithelial systems (25, 37) indicate that net vectorial transport depends critically on ENaC and CFTR operating in concert with the tight junctions. Fluid absorption is mainly controlled by the transport of Na down its electrochemical gradient through apical ENaC, while fluid secretion is regulated by cell-to-lumen movement of Cl and/or HCO_3 through cAMP-stimulated CFTR (and perhaps also by inactivation of ENaC, see below). In both cases, the obligatory movement of counterions (cations to accompany active Cl secretion and anions to accompany active Na absorption) likely takes place predominantly through leaky tight junctions driven by the basal side-positive TEP. Thus, "leaky" tight junctions are important for the ability of an epithelium to exhibit both absorption and secretion.

The net balance between secretion and absorption in 31EG4 cells may be determined in large part by the activity of CFTR in the apical membrane. This idea is consistent with the observation that fluid absorption increases monotonically with R_T, and the cAMP-induced alteration in J_V is smallest for control tissues that secreted fluid and largest for control tissues that absorbed fluid (Fig. 15). Thus, when CFTR conductance is lowest, R_T is highest and the monolayers absorb Na, Cl and fluid. Subsequent elevation of cell cAMP could then activate the

maximum number of CFTR channels and produce the maximum alteration in J_V (Fig. 15). Conversely, cultures that have a relatively low R_T may have a relatively large complement of active CFTR in the apical membrane and therefore secrete fluid in the basal state (Fig. 15); secretion is increased by amiloride block of ENaC (Fig. 14).

The tight junctions will also play a role in determining secretion *vs* absorption because the intraepithelial current ($i = TEP/R_S$) (32), determined in part by the low resistance of the junctions ($R_S < R_A + R_B$), hyperpolarizes V_A, thereby increasing Na entry (ENaC) into and Cl (CFTR) exit from the cells. During cAMP stimulation V_a depolarizes by 18 mV (Table 1) and the increase in fluid secretion indicates that the net electrochemical gradient for Cl is outward across the apical membrane.

These considerations emphasize the importance of the integrated activities of ion channels, tight junctions and ion transporters in determining the direction of net Cl movement through CFTR. They also suggest a functional distinction among epithelia with apical ENaC and CFTR. Epithelia with tight junctions that are essentially impermeable to ions can only absorb salts and fluid *via* the cellular pathway. In these tissues, the shunt current is zero and V_A is sufficiently depolarized such that the electrochemical driving forces for both Cl and Na are inward across the apical membrane. Therefore, activation of CFTR with cAMP elicits absorption of Cl, Na, and fluid through the cells[2]. Examples include human sweat ducts and bovine trachea (38, 46) and may also be true in the lactating mammary gland which has large lumen negative TEP (-35 mV), characteristic of all tight epithelia, and low concentrations of Na and Cl in the milk (35).

In contrast, epithelia like 31EG4 cells that have relatively leaky junctions generate a shunt current that hyperpolarizes V_A, increasing Cl exit (CFTR) and Na entry (ENaC) across the apical membrane. The conductance of the shunt to anions and cations and the existence of a TEP permit these cells to either secrete or absorb salts and fluid depending on the ratio of g_{ENaC}/g_{CFTR} and on the direction and magnitude of the electrochemical driving forces for these ions across the apical membrane. This appears also to be the case in airway submucosal glands. When CFTR is

activated, these cells secrete fluid driven by the transport of HCO_3 and Cl through CFTR (2, 23, 45) with Na following through ion-permeable tight junctions to maintain electroneutrality. In cystic fibrosis, when CFTR is inactive, submucosal gland cells absorb Na (through ENaC), Cl (through the paracellular pathway) and fluid (25). This capability to both secrete and absorb fluids may also be characteristic of the non-lactating mammary gland (with its leaky tight junctions) (35).

Effects of cAMP on CFTR and ENaC: evidence for cross talk?

A number of observations indicated that cAMP-activated CFTR inhibited ENaC. Cyclic AMP caused, in addition to the expected increase in CFTR activity and consequent drop in R_T and R_A, an almost complete inhibition of the amiloride-induced changes in TEP, R_T, R_A/R_B and R_A (Fig. 12B; Tables 1B,C and 2B,C). The amiloride-induced voltage responses may have been decreased because cAMP depolarized the apical membrane and reduced the driving force for Na entry, but similar inhibitory effects were seen in other experiments (not shown) in which the apical membrane was current-clamped close to its resting level in the absence of cAMP. Of course E_{Na} might have been reduced by this maneuver, but the more than ten-fold reduction in the amiloride-induced changes in R_T and R_A/R_B suggests that CFTR activation inhibited ENaC.

Experiments comparing the electrical responses of ATP and cAMP similarly indicated that the apparent inhibition of ENaC by CFTR is not due to an electrophysiological effect. ATP and cAMP have practically identical effects on membrane voltage but very different effects on the amiloride–induced changes in TEP and R_T. Fig 12 and Tables 2,3 show that the amiloride responses are very similar to control in the presence of ATP but almost totally absent in the presence of cAMP. In addition, the data and calculations in summarized in Tables 1 and 2 allowed us to calculate the amiloride-induced change in apical membrane Na conductance (Δg_{Na}) in control Ringer and when CFTR is activated by cAMP. By definition, $1/R_A = g_{Na} + g_{Cl} + g_x$ where the subscripts indicate the apical membrane conductances for Na, Cl and unidentified channels X (likely including K channels-unpublished data). Similarly, $1/R_A^* = g_{Na}^* + g_{Cl} + g_x$

after amiloride and $1/R_A - 1/R_A^* = g_{Na} - g_{Na}^* = \Delta g_{Na}$. Using data in Table 1C, we calculate that amiloride decreased g_{Na} by 0.35 mS/cm^2 in control Ringer but had no effect in the presence of cAMP. Although ATP and cAMP have nearly identical effects in reducing R_A, ATP stimulation of Ca^{2+}-activated Cl channels has essentially no apparent inhibitory effect on ENaC but cAMP stimulation of CFTR appears to totally block ENaC, a conclusion previously reached for some (27, 43), but not all (38), preparations.

TEXT FOOTNOTES

[1] In a comparison of six, eight and 14 day old cultures from the same set of cells the mean (± SEM) J_V was: – 0.9 ± 1.6 $\mu l \cdot cm^{-2} \cdot hr^{-1}$ (n = 8; 4 absorbing), -2.6 ± 0.8 $\mu l \cdot cm^{-2} \cdot hr^{-1}$ (n = 9; 3 absorbing), -3.3 ± 2.9 $\mu l \cdot cm^{-2} \cdot hr^{-1}$ (n = 11; 3 absorbing), respectively. These values are not statistically different from each other ($p > 0.3$).

[2] In two experiments (not shown) net fluid absorption was increased by cAMP. As expected, cAMP decreased R_T in these two experiments, but TEP also decreased which is opposite to the results obtained in all the other experiments. This suggests that the electrochemical gradient for Cl was inward in these two cases as previously shown in bovine trachea (Uyekubo et al., 1998).

ACKNOWLEDGEMENTS

This work was supported by grants from the Department of the Army Breast Cancer Research Program DAMD17-96-1-6315 (SM), DAMD17-97-5231 (TM), California Breast Cancer Research Program 5JB-0077 (SM), and NIH DK51799 (TM). We thank Connie Yu for help with experiments summarized in Figure 6; Van Nguyen, Steve Jalickee, and Natalia Zhuravel for experiments summarized in Figure 14. It is our pleasure to thank Beate Illek, Horst Fischer, and Jonathan Widdicombe for their helpful comments on an earlier version of the manuscript. We are also grateful to Pascal Barbry and Genzyme (John Marshall) for supplying antibodies.

REFERENCES

1. Angeli, A. D., L; Naldoni, C; Orlandi, F; Puligheddu, B; Caraci, P; Bucchi, L; Torta, M; Bruzzi, P. Steroid biochemistry and categorization of breast cyst fluid: relation to breast cancer risk. *Journal of Steroid Biochemistry and Molecular Biology.* 49(4-6): 333-9, 1994.

2. Ballard, S. T., L. Trout, Z. Bebok, E. J. Sorscher, and A. Crews. CFTR involvement in chloride, bicarbonate, and liquid secretion by airway submucosal glands [In Process Citation]. *Am J Physiol* 277: L694-9, 1999.

3. Bisbee, C. A. Alterations in electrophysiology of cultured BALB/cfC3H mouse mammary epithelium associated with neoplastic transformation. *Cancer Lett* 14: 237-42, 1981.

4. Bisbee, C. A., T. E. Machen, and H. A. Bern. Mouse mammary epithelial cells on floating collagen gels: transepithelial ion transport and effects of prolactin. *Proc Natl Acad Sci U S A* 76: 536-40, 1979.

5. Bodian, C. A. Benign breast diseases, carcinoma in situ, and breast cancer risk. *Epidemiol Rev* 15: 177-87, 1993.

6. Bodian, C. A., R. lattes, and K. H. Perzin. The epidemiology of gross cystic disease of the breast confirmed by biopsy or by aspiration of cyst fluid. *Cancer Detect Prev* 16: 7-15, 1992.

7. Boucher, R. C. Human airway ion transport. Part one. *Am J Respir Crit Care Med* 150: 271-81, 1994.

8. Bundred, N. J., R. R. West, J. O. Dowd, R. E. Mansel, and L. E. Hughes. Is there an increased risk of breast cancer in women who have had a breast cyst aspirated? *Br J Cancer* 64: 953-5, 1991.

9. Caputo, E., G. Manco, L. Mandrich, and J. Guardiola. A novel aspartyl proteinase from apocrine epithelia and breast tumors. *J Biol Chem* 275: 7935-41, 2000.

10. Ciatto, S., A. Biggeri, M. Rosselli Del Turco, D. Bartoli, and A. Iossa. Risk of breast cancer subsequent to proven gross cystic disease. *Eur J Cancer* 26: 555-7, 1990.

11. Cohn, J. A., O. Melhus, L. J. Page, K. L. Dittrich, and S. R. Vigna. CFTR: development of high- affinity antibodies and localization in sweat gland. *Biochem Biophys Res Commun* 181: 36-43, 1991.

12. Cohn, J. A., A. C. Nairn, C. R. Marino, O. Melhus, and J. Kole. Characterization of the cystic fibrosis transmembrane conductance regulator in a colonocyte cell line. *Proc Natl Acad Sci U S A* 89: 2340-4, 1992.

13. Cohn, J. A., T. V. Strong, M. R. Picciotto, A. C. Nairn, F. S. Collins, and J. G. Fitz. Localization of the cystic fibrosis transmembrane conductance regulator in human bile duct epithelial cells. *Gastroenterology1* 05: 1857-64, 1993.

14. Diamond, J. M. Channels in epithelial cell membranes and junctions. *Fed Proc* 37: 2639-43, 1978.

15. Dick, G. M., I. D. Kong, and K. M. Sanders. Effects of anion channel antagonists in canine colonic myocytes: comparative pharmacology of Cl-, Ca2+ and K+ currents. *Br J Pharmacol* 127: 1819-31, 1999.

16. Dixon, J. M., C. McDonald, R. A. Elton, and W. R. Miller. Risk of breast cancer in women with palpable breast cysts: a prospective study. Edinburgh Breast Group [see comments]. *Lancet* 353: 1742-5, 1999.

17. Dogliotti, L., F. Orlandi, P. Caraci, B. Puligheddu, M. Torta, and A. Angeli. Biochemistry of breast cyst fluid. An approach to understanding intercellular communication in the terminal duct lobular units. *Ann N Y Acad Sci* 586: 17-28, 1990.

18. Engelhardt, J. F., J. R. Yankaskas, S. A. Ernst, Y. Yang, C. R. Marino, R. C. Boucher, J. A. Cohn, and J. M. Wilson. Submucosal glands are the predominant site of CFTR expression in the human bronchus. *Nat Genet* 2: 240-8, 1992.

19. Firsov, D., M. Robert-Nicoud, S. Gruender, L. Schild, and B. C. Rossier. Mutational analysis of cysteine-rich domains of the epithelium sodium channel (ENaC). Identification of cysteines essential for channel expression at the cell surface. *J Biol Chem* 274: 2743-9, 1999.

20. Grubb, B. R., and R. C. Boucher. Enhanced colonic Na+ absorption in cystic fibrosis mice versus normal mice. *Am J Physiol* 272: G393-400, 1997.

21. Haagensen, C. D. The relationship of gross cystic disease of the breast and carcinoma [editorial]. *Ann Surg* 185: 375-6, 1977.

22. Hughes, B. A., S. S. Miller, and T. E. Machen. Effects of cyclic AMP on fluid absorption and ion transport across frog retinal pigment epithelium. Measurements in the open-circuit state. *Journal of General Physiology* 83: 875-99, 1984.

23. Inglis, S. K., M. R. Corboz, A. E. Taylor, and S. T. Ballard. Effect of anion transport inhibition on mucus secretion by airway submucosal glands. *Am J Physiol* 272: L372-7, 1997.

24. Jiang, C., W. E. Finkbeiner, J. H. Widdicombe, P. B. McCray, Jr., and S. S. Miller. Altered fluid transport across airway epithelium in cystic fibrosis. *Science* 262: 424-7, 1993.

25. Jiang, C., W. E. Finkbeiner, J. H. Widdicombe, and S. S. Miller. Fluid transport across cultures of human tracheal glands is altered in cystic fibrosis. *Journal of Physiology* 501: 637-647, 1997.

26. Joseph, D. P., and S. S. Miller. Apical and basal membrane ion transport mechanisms in bovine retinal pigment epithelium. *J Physiol (Lond)* 435: 439-63, 1991.

27. Kunzelmann, K., G. L. Kiser, R. Schreiber, and J. R. Riordan. Inhibition of epithelial Na+ currents by intracellular domains of the cystic fibrosis transmembrane conductance regulator. *FEBS Lett* 400: 341-4, 1997.

28. Leis, H. P., Jr. The role of tamoxifen in the prevention and treatment of benign and malignant breast lesions: a chemopreventive. *Int Surg* 78: 176-82, 1993.

29. Linzell, J., M. Peaker, and J. Taylor. The effects of prolactin and oxytocin on milk secretion and on the permeability of the mammary epithelium in the rabbit. *Journal of Physiology* 253: 547-563, 1975.

30. Malatesta, M., F. Mannello, M. Sebastiani, A. Cardinali, F. Marcheggiani, F. Reno, and G. Gazzanelli. Ultrastructural characterization and biochemical profile of human gross cystic breast disease. *Breast Cancer Res Treat* 48: 211-9, 1998.

31. Marino, C. R., L. M. Matovcik, F. S. Gorelick, and J. A. Cohn. Localization of the cystic fibrosis transmembrane conductance regulator in pancreas. *Journal of Clinical Investigation* 88: 712-716, 1991.

32. Miller, S. S., and R. H. Steinberg. Passive ionic properties of frog retinal pigment epithelium. *J Membr Biol* 36: 337-72, 1977.

33. Molina, R., X. Filella, M. Herranz, M. Prats, A. Velasco, G. Zanon, M. J. Martinez-Osaba, and A. M. Ballesta. Biochemistry of cyst fluid in fibrocystic disease of the breast. Approach to classification and understanding of the mechanism of formation. *Ann N Y Acad Sci* 586: 29-42, 1990.

34. Neville, M. C. The physiological basis of milk secretion. *Ann N Y Acad Sci* 586: 1-11, 1990.

35. Nguyen, D. A., and M. C. Neville. Tight junction regulation in the mammary gland. *J Mammary Gland Biol Neoplasia* 3: 233-46, 1998.

36. Peterson, W., C. Meggyesy, K. Yu, and S. S. Miller. Extracellular ATP activates calcium signaling, ion and fluid transport in retinal pigment epithelium. *The Journal of Neuroscience* 17: 2324-2337, 1997.

37. Peterson, W. M., J. N. Quong, and S.S.Miller. Mechanisms of fluid transport in retinal pigment epithelium. *The Third Great Basin Visual Science Symposium on Retinal Research* III: 34 - 42, 1998.

38. Reddy, M. M., M. J. Light, and P. M. Quinton. Activation of the epithelial Na+ channel (ENaC) requires CFTR Cl- channel function. *Nature* 402: 301-4, 1999.

39. Reichmann, E., R. Ball, B. Groner, and R. R. Friis. New mammary epithelial and fibroblastic cell clones in coculture form structures competent to differentiate functionally. *J Cell Biol* 108: 1127-38, 1989.

40. Schultz, B. D., A. K. Singh, D. C. Devor, and R. J. Bridges. Pharmacology of CFTR chloride channel activity. *Physiological Reviews* 79, Suppl.: 109-144, 1999.

41. Sjaastad, M. D., K. S. Zettl, G. Parry, G. L. Firestone, and T. E. Machen. Hormonal regulation of the polarized function and distribution of Na/H exchange and Na/HCO3 cotransport in cultured mammary epithelial cells. *J Cell Biol* 122: 589-600, 1993.

42. Strange, R., F. Li, R. R. Friis, E. Reichmann, B. Haenni, and P. H. Burri. Mammary epithelial differentiation in vitro: minimum requirements for a functional response to hormonal stimulation. *Cell Growth Differ* 2: 549-59, 1991.

43. Stutts, M. J., C. M. Canessa, J. C. Olsen, M. Hamrick, J. A. Cohn, B. C. Rossier, and R. C. Boucher. CFTR as a cAMP-dependent regulator of sodium channels [see comments]. *Science* 269: 847-50, 1995.

44. Stutts, M. J., B. C. Rossier, and R. C. Boucher. Cystic fibrosis transmembrane conductance regulator inverts protein kinase A-mediated regulation of epithelial sodium channel single channel kinetics. *J Biol Chem* 272: 14037-40, 1997.

45. Trout, L., M. King, W. Feng, S. K. Inglis, and S. T. Ballard. Inhibition of airway liquid secretion and its effect on the physical properties of airway mucus. *Am J Physiol* 274: L258-63, 1998.

46. Uyekubo, S. N., H. Fischer, A. Maminishkis, B. Illek, S. S. Miller, and J. H. Widdicombe. cAMP-dependent absorption of chloride across airway epithelium. *Am J Physiol* 275: L1219-27, 1998.

47. von Weikersthal, S. F., M. A. Barrand, and S. B. Hladky. Functional and molecular characterization of a volume-sensitive chloride current in rat brain endothelial cells. *J Physiol (Lond)* 516: 75-84, 1999.

48. Zettl, K. S., M. D. Sjaastad, P. M. Riskin, G. Parry, T. E. Machen, and G. L. Firestone. Glucocorticoid-induced formation of tight junctions in mouse mammary epithelial cells in vitro. *Proc Natl Acad Sci U S A* 89: 9069-73, 1992.

TABLE LEGENDS

Table 1. Summary of electrophysiological data from control, cAMP and amiloride treated tissues. **A.** Control data. **B.** Amiloride, 20 μM (row 1) and cAMP (row 2) induced changes in membrane voltage and resistance. **C.** Equivalent circuit parameters calculated from the control data (**A**) and from the electrical changes induced by adding amiloride to control Ringer (**B**, top line). Calculated values of R_A, R_B, R_S, E_A, and E_B in control and in the presence of amiloride are shown in top and bottom lines, respectively. Differences between control and cAMP and control and amiloride are significant in all cases ($p < 0.01$). Star symbol (*) signifies the assumption that R_B and R_S are not altered by apical amiloride.

Table 2. **A.** Steady-state levels of membrane voltage and resistance in the presence of cAMP. **B.** The amiloride responses in the presence of cAMP. **C.** An equivalent circuit analysis, rows 1 & 2, (similar to that in **Table 1)** was carried out to compare the amiloride-induced changes in apical membrane resistance and electromotive force in the absence and presence of cAMP. The steady-state values in cAMP plus amiloride are not significantly different from those in cAMP alone ($n = 6$; paired t-test).

Table 3. Comparison of effects of cAMP, ATP and amiloride on TEP and R_T. **A.** Row 1, control TEP and R_T measurements of 31EG4 monolayers ($n=12$, ± SEM). Rows 2 and 3 show that the ATP- and cAMP- induced changes in TEP and R_T were statistically indistinguishable. **B.** Row 1, amiloride-induced changes in TEP and R_T. Rows 2 and 3, amiloride induced changes in the presence of ATP ($n=7$) or cAMP ($n=6$), respectively. The amiloride-induced changes in TEP and R_T in the presence of cAMP were significantly reduced compared to the changes observed in control or in ATP ($p < 0.001$).

FIGURE LEGENDS

Fig 1. Equivalent circuit for 31EG4 mammary epithelia. Apical and basolateral membranes are represented by equivalent resistance, R_A or R_B, respectively, in series with an electromotive force, E_A or E_B, that would be measured in the absence of a shunt. Shunt resistance, R_S, represents the parallel combination of the junctional complex resistance and the mechanical seal resistance around the tissue. A loop current, i_s, flows through the circuit due to the difference between V_A and V_B. The measured apical and basolateral membrane voltages are represented as V_A and V_B, respectively. The transepithelial potential, TEP, represents the difference between V_B and V_A.

Fig 2. PCR products for ENaC (596 bp) and CFTR (463 bp). The amplified products were run on a 1.5% agarose gel and stained with ethidium bromide. The 100 base pair ladder is on the left (Ladder).

Fig 3. Western blot analysis of CFTR and ENaC protein in 31EG4 cells. Cell homogenates were loaded for SDS-PAGE and analyzed subsequently by Western blotting. The migration of molecular mass markers (kDa) is indicated. See text for details.

Fig 4. Immunofluorescence localization of ENaC (**A**) and CFTR (**C**) and their respective bright field images (**B**) and (**D**) in a 31EG4 monolayer. Cryostat sections were stained with primary antibodies to the β subunit of ENaC and to CFTR and then FITC-conjugated with secondary antibodies. The transwell mesh is visible below the monolayer (**B, D**). Staining with primary antibodies showed that both ENaC (**A**) and CFTR (**C**) were located in the apical regions of the cells. Original magnifications were 630x.

Fig. 5. Detection of CFTR and cytokeratin 19 in intact human breast by double-label indirect immunofluorescence with a1468 plus a monoclonal antibody to cytokeratin 19. The upper panel shows a1468 staining of the apical domain of ductal epithelial cells as detected from the FITC

(green) fluorescence. The lower panel shows the combined fluorescence with both antibodies in a double exposure showing fluorescence. The TRITC fluorescence (orange-red) identifies duct cells based on their content of cytokeratin 19. The FITC fluorescence (green) occurs at the apical domain of these duct cells. Original magnification, 400X.

Fig. 6. Effects of amiloride, forskolin and DPC on I_{SC} of 31EG4 monolayers. Cells grown to confluency on filters were mounted in the chamber and I_{SC} was measured. Spikes in I_{SC} trace represent changes induced by briefly clamping epithelium to 5 mV. Apical addition of amiloride caused I_{SC} to decrease from about 13.5 $\mu A/cm^2$ to 11.5 $\mu A/cm^2$. Subsequent treatment with 10 μM forskolin (to increase cAMP) caused I_{SC} to increase from 13.5 $\mu A/cm^2$ to 15 $\mu A/cm^2$, and DPC reduced I_{SC} to 9 $\mu A/cm^2$. Experiment is typical of four others.

Fig. 7. Effects of forskolin and DPC on whole cell patch clamp current, I-V relationship and conductance. **A**. Whole cell I-V recording of a resting cell with a basal Cl conductance of 1.7 nS and reversal potential of -20 mV. Upon addition of forskolin, conductance increased to 34 nS, and the reversal potential shifted to -25 mV. Addition of 2 mM DPC decreased the conductance to 2.7 nS and shifted reversal potential back to - 20 mV. **B**. Summary of 7 similar experiments. Average whole cell conductance of resting cells was 3.4 $\pm$1.2 nS, stimulated conductance was 27.4 $\pm$ 4.1 nS and after DPC conductance was 2.7 $\pm$0.6 nS.

Fig. 8. Effect amiloride on whole cell patch clamp current, I-V relationship and conductance in NaCl and Na gluconate Ringer's. **A**. Whole cell patch recording of a resting cell with a basal conductance in NaCl solution of 0.6 nS and reversal potential of -15 mV. 10 μM amiloride caused conductance to decrease to 0.3 nS and shifted the reversal potential to -22 mV. **B**. Summary of two experiments performed with NaCl bathing solutions (filled circles) and two experiments performed with Na gluconate solutions (open circles). Average resting conductance

was 1.2 nS in NaCl solution and 0.7 nS after amiloride. Average resting conductance in Na gluconate solution was 16.5 nS, decreasing to 8.8 nS after amiloride.

Fig. 9. Effects of cAMP cocktail on membrane voltage and resistance in 31EG4 cells. The horizontal black bar at the bottom indicates the length of time the cAMP cocktail was added to the apical chamber. **Top panel**: Continuous traces represent V_A and V_B, as labeled, and open circles represent the ratio of apical to basolateral membrane resistance, R_A/R_B. The cAMP-elevating cocktail (see Methods) caused, after a brief delay, depolarizations of both V_A and V_B by > 10 mV while R_A/R_B decreased. **Bottom panel**: TEP (continuous trace) increased by 2 mV, R_T (open squares) decreased by 200 $\Omega \cdot cm^2$ and R_A/R_B decreased by approximately a factor of two, from 3.4 to 1.7. These results are consistent with cAMP opening Cl channels in the apical membrane.

Fig. 10. Cyclic AMP-induced changes in membrane voltage and resistance are blocked by NPPB in 31EG4 cells. **Top panel**: Continuous traces represent V_A and V_B, as labeled, and open circles represent R_A/R_B. **Bottom panel**: Continuous trace represents TEP, and open squares represent R_T. In the presence of NPPB, the cAMP cocktail elicited only small electrophysiological responses. Removal of NPPB caused V_A and V_B to depolarize by > 10 mV, while TEP increased and R_T and R_A/R_B both decreased.

Fig. 11. Amiloride-induced changes in membrane voltage and resistance. **Top panel**: Continuous traces represent V_A and V_B, as labeled, and open circles represent the ratio of apical to basolateral membrane resistance, R_A/R_B. In control Ringer, V_A = -46 mV. Apical amiloride (20 μM) hyperpolarized V_A by 24 mV; R_A/R_B increased by approximately a factor of six. **Bottom panel**: TEP (continuous trace) decreased by 2 mV, and R_T (open squares) increased by 100 $\Omega \cdot cm^2$. Effects of amiloride were readily reversed upon removal from the apical bath.

Fig. 12. Amiloride - induced changes in membrane voltage and resistance in the absence and presence of cAMP-elevating cocktail. **A.** Amiloride caused characteristic changes in V_A, V_B, R_A/R_B, TEP and R_T, and subsequent addition of cAMP cocktail in the continued presence of amiloride produced cAMP responses similar to those measured in control Ringer (Table 1B). **B.** 31EG4 cells were first treated with cAMP cocktail, which caused characteristic depolarization of V_A, decrease of R_A/R_B, and increase in TEP. Subsequent addition of amiloride in the continued presence of cAMP produced no significant changes in R_T, R_A/R_B or TEP and V_A. Summary data in Table 1B. **C.** Amiloride – induced changes in TEP and R_T in the presence and absence of cAMP or ATP were measured in the *same monolayer*. In the top panel, control TEP and R_T were -5.5 mV and 950 $\Omega \cdot cm^2$, respectively. Apical amiloride reversibly decreased TEP (1.5 mV) and increased R_T (125 $\Omega \cdot cm^2$). The tissue was returned to control Ringer and then cAMP cocktail was added to the apical bath; TEP increased by 1.7 mV and R_T decreased by 110 $\Omega \cdot cm^2$. In the presence of cAMP, apical amiloride produced no changes in TEP or R_T. The monolayer was then returned to control Ringer (30 min); TEP and R_T returned to their control levels. Apical ATP increased TEP (2 mV) and decreased R_T (200 $\Omega \cdot cm^2$). In the presence of ATP, apical amiloride reversibly decreased TEP by 1 mV and increased R_T by 75 $\Omega \cdot cm^2$. Subsequent ATP removal decreased TEP and increased R_T.

Fig. 13. Cyclic AMP - induced stimulation of steady-state fluid secretion. Apical addition of the cAMP cocktail reversed the direction of net steady-state fluid transport from absorption (3.5 $\mu l \cdot cm^{-2} \cdot hr^{-1}$) to secretion (–3.0 $\mu l \cdot cm^{-2} \cdot hr^{-1}$) and simultaneously increased TEP and decreased R_T consistent with the electrophysiological responses summarized in Table 1B. The obligatory control-to-control solution change (probes out, see Methods) during the first 40 min produced very little change in J_V, TEP, and R_T. Removal of cAMP from the apical bath brought J_V back to absorption at $\approx$ 1.0 $\mu l \cdot cm^{-2} \cdot hr^{-1}$. The electrical changes were also reversible.

Fig. 14. Summary of fluid transport experiments with cAMP (n=11) or amiloride (n=6) addition. A subset of monolayers (n = 9) absorbed fluid at a mean J_v of 3.6 ± 1.1 $\mu l \cdot cm^{-2} \cdot hr^{-1}$ Another subset of cultures (n = 8) secreted fluid at a mean rate of -4.6 ± 0.8 $\mu l \cdot cm^{-2} \cdot hr^{-1}$. both cAMP and amiloride induced fluid secretion.

Fig. 15. Magnitude of cAMP- induced fluid secretory response (ΔJ_v) and R_T are plotted as a function of baseline, steady-state Jv in 31EG4 cells. Cyclic AMP -induced fluid secretion rate and R_T increase linearly (as net fluid absorption rate increases). The correlation coefficients, 0.6 and 0.8, respectively, are statistically significant ($p < 0.01$)

Table 1

A.	TEP (mV)	R_T ($\Omega \cdot cm^2$)	V_A (mV)	V_B (mV)	R_A/R_B
Untreated (n=32)	-5.9 ± .51	828.9 ± 53.9	-40.7 ± 1.5	-46.6 ± 1.6	2.8 ± 0.23

B.	ΔTEP (mV)	Δ R_T ($\Omega \cdot cm^2$)	Δ V_A (mV)	Δ V_B (mV)	Δ[R_A/R_B]
+ Amiloride (n=16)	+3.1 ±0.45	+137.2 ± 18.5	-19.7 ± 1.39	-16.9 ± 1.49	+5.8 ± 0.49
+ cAMP (n=20)	-2.2 ± 0.14	-155.5 ± 14.8	+17.6 ± 1.0	+15.4 ± 1.0	-1.7 ± 0.18

C. Equivalent Circuit Calculations

	R_A ($\Omega \cdot cm^2$)	R_B ($\Omega \cdot cm^2$)	R_s ($\Omega \cdot cm^2$)	E_A (mV)	E_B (mV)
Control	1958.9 ± 298.2	776.4* ± 110.3	958.9* ± 93.8	-27.9 ± 2.0	-48.4 ± 2.4
+ Amiloride (n=16)	6550.2 ± 763.6	776.4* ± 110.3	958.9* ± 93.8	-67.9 ± 4.0	-64.3 ± 2.7

Table 2

A.

	TEP (mV)	R_T ($\Omega \cdot cm^2$)	V_A (mV)	V_B (mV)	R_A/R_B
cAMP (n=6)	-5.9 ±0.2	563.3 ± 86.0	-20.33 ± 2.3	-25.53 ± 2.2	0.25 ± 0.03

B.

	ΔTEP (mV)	Δ R_T ($\Omega \cdot cm^2$)	Δ V_A (mV)	Δ V_B (mV)	Δ[R_A/R_B]
cAMP + Amiloride (n=6)	0.0 ± 0.0	+8.8 ± 3.0	-2.3 ± 0.6	-2.3 ± 0.6	+0.03 ± 0.005

C. Equivalent Circuit Calculations

	R_A ($\Omega \cdot cm^2$)	R_B ($\Omega \cdot cm^2$)	R_s ($\Omega \cdot cm^2$)	E_A (mV)	E_B (mV)
cAMP (n=6)	157.4 ±26.4	760.2* ± 139.8	1848.6* ± 426.6	-19.7 ± 2.4	-28.8 ±1.6
cAMP + Amiloride (n=6)	178.8 ± 26.4	760.2* ± 139.8	1848.6* ± 426.6	-22.0 ± 2.7	-31.11 ± 1.8

Table 3

A.	TEP (mV)	R_T ($\Omega \cdot cm^2$)
Control (n=12)	-4.44 ±0.49	674.7 ± 51.6
	ΔTEP (mV)	**Δ R_T ($\Omega \cdot cm^2$)**
+ATP (n=7)	-2.0 ±0.36	-121 ± 14.8
+cAMP (n=6)	-1.9 ±0.34	-110 ± 9.4

B.	ΔTEP (mV)	ΔR_T ($\Omega \cdot cm^2$)
Control + Amiloride (n=12)	+0.99 ±0.08	+90.5 ± 8.6
ATP + Amiloride (n=7)	+0.69 ±0.04	+69.8 ± 10.7
cAMP + Amiloride (n=6)	+0.03 ±0.02	+7.7 ± 1.7

FIGURE 1

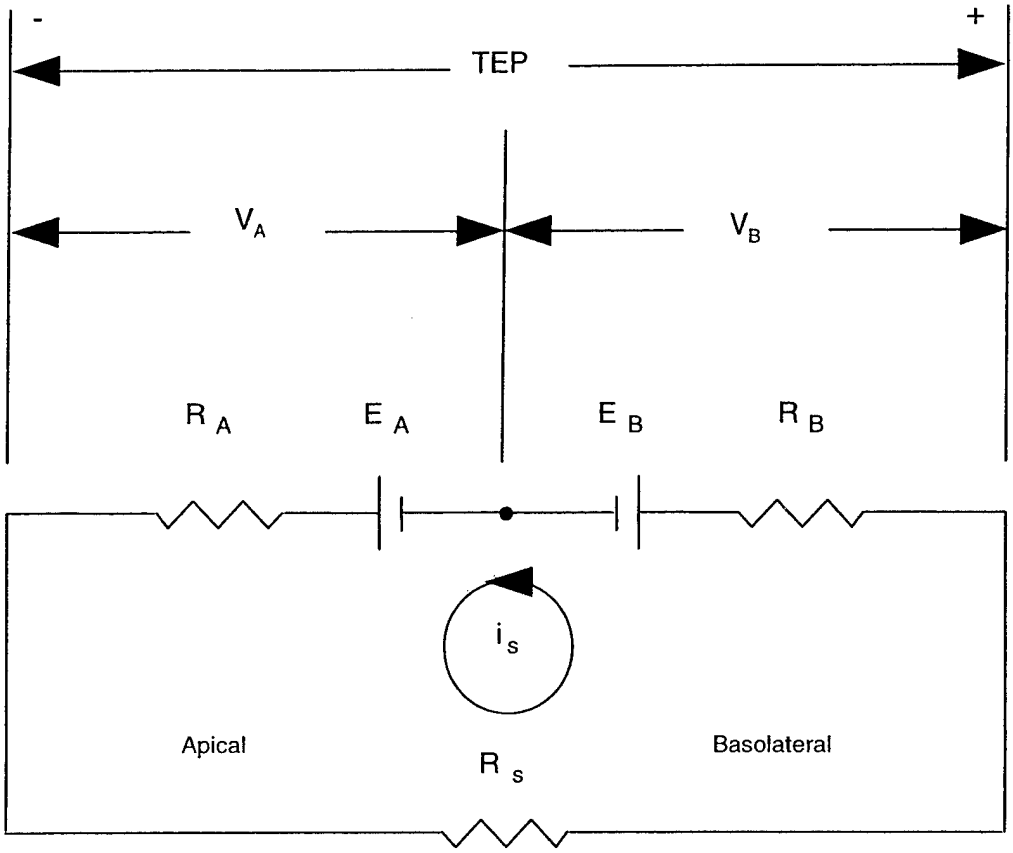

β-ENaC
CFTR
170 kDa
85 kDa

A

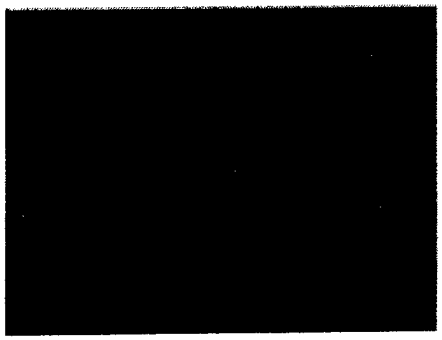

C

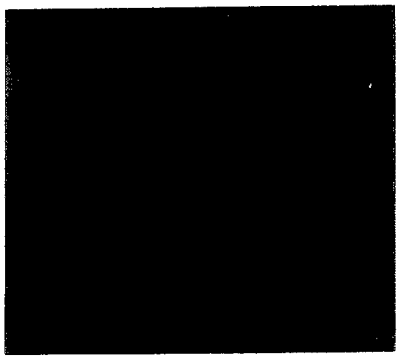

B

D

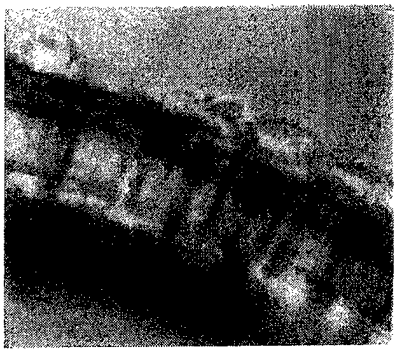

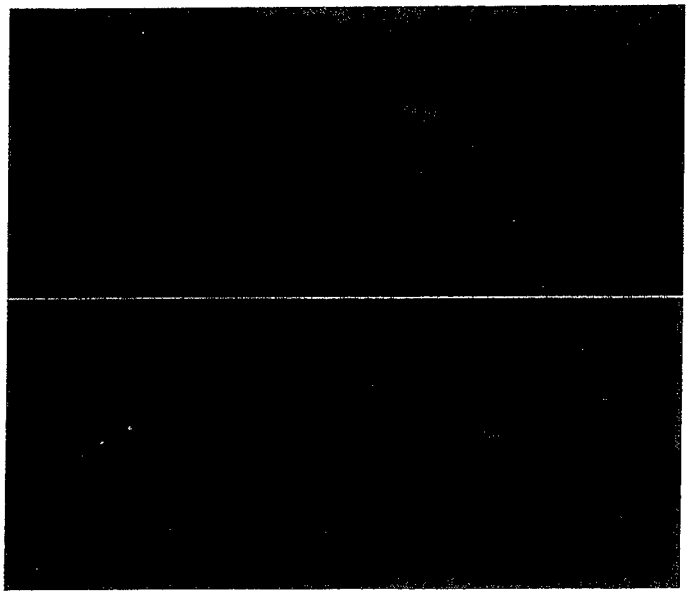

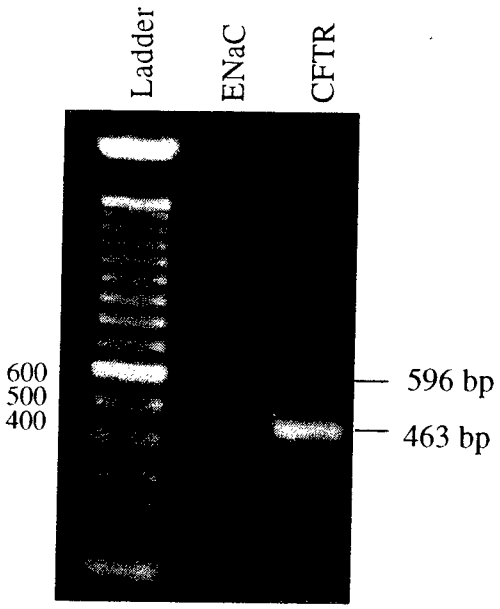
Ladder
ENaC
CFTR
600
500
400
596 bp
463 bp

FIGURE 6

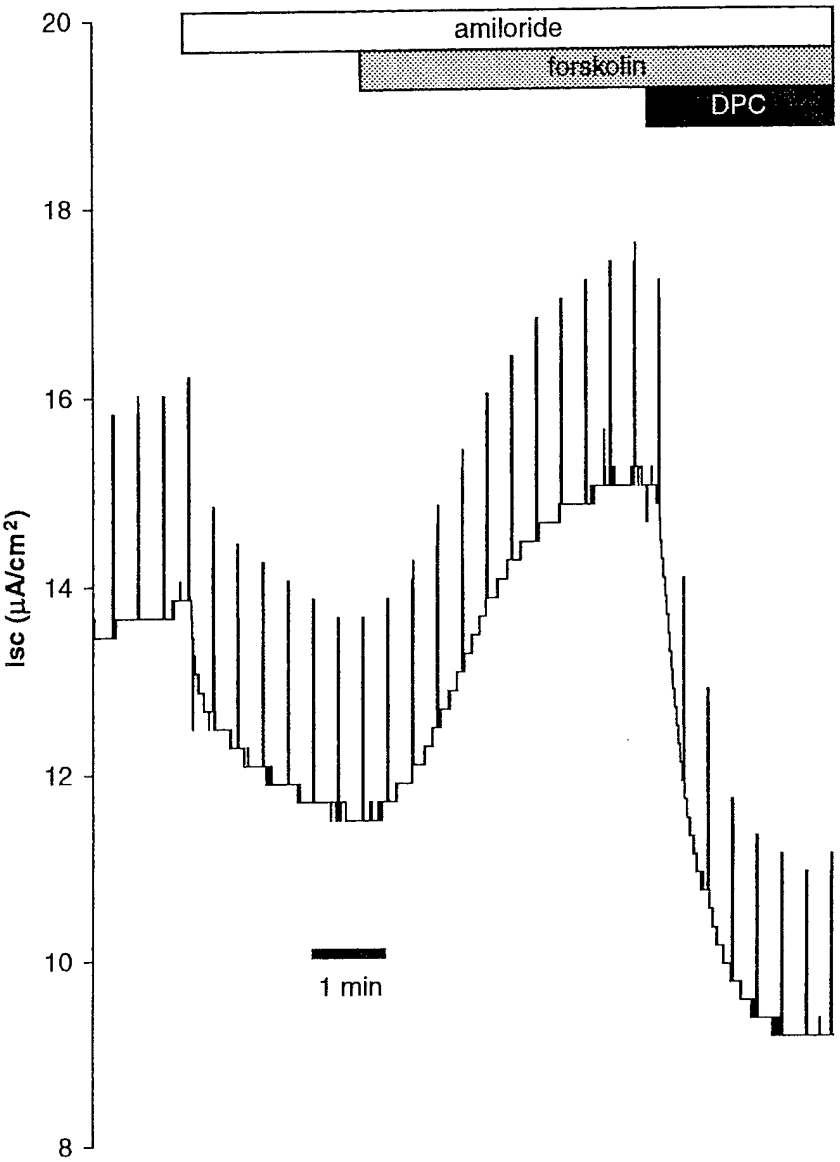

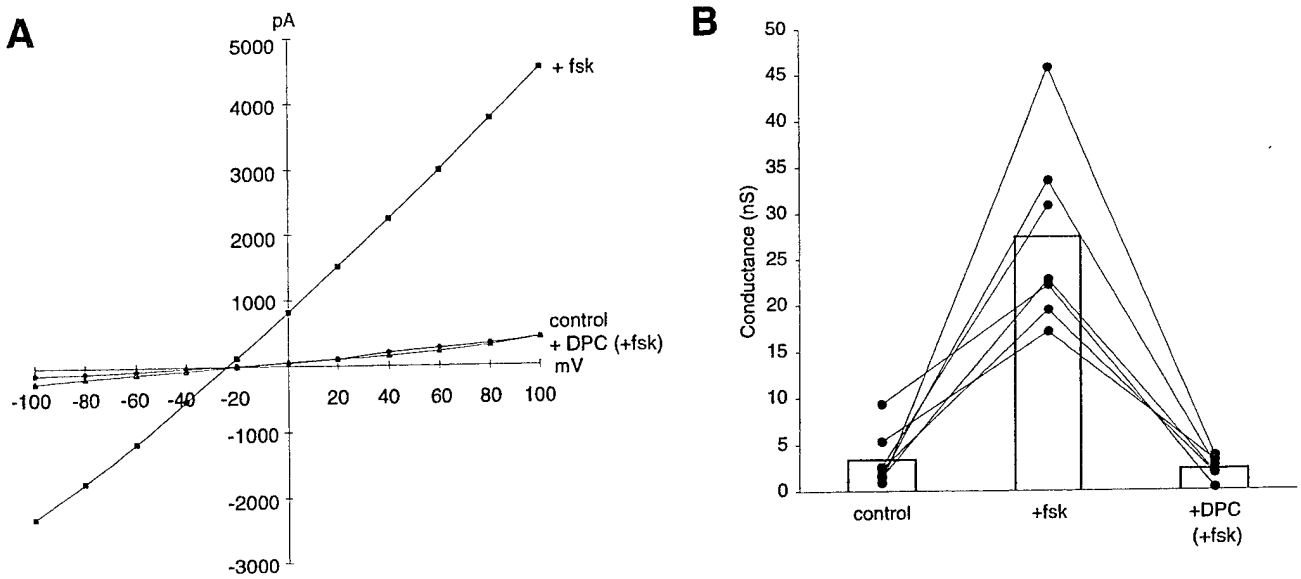
A
pA
5000
4000
3000
2000
1000
-1000
-2000
-3000
+ fsk
control
+ DPC (+fsk)
mV
-100
-80
-60
-40
-20
20
40
60
80
100
B
Conductance (nS)
50
45
40
35
30
25
20
15
10
5
0
control
+fsk
+DPC
(+fsk)

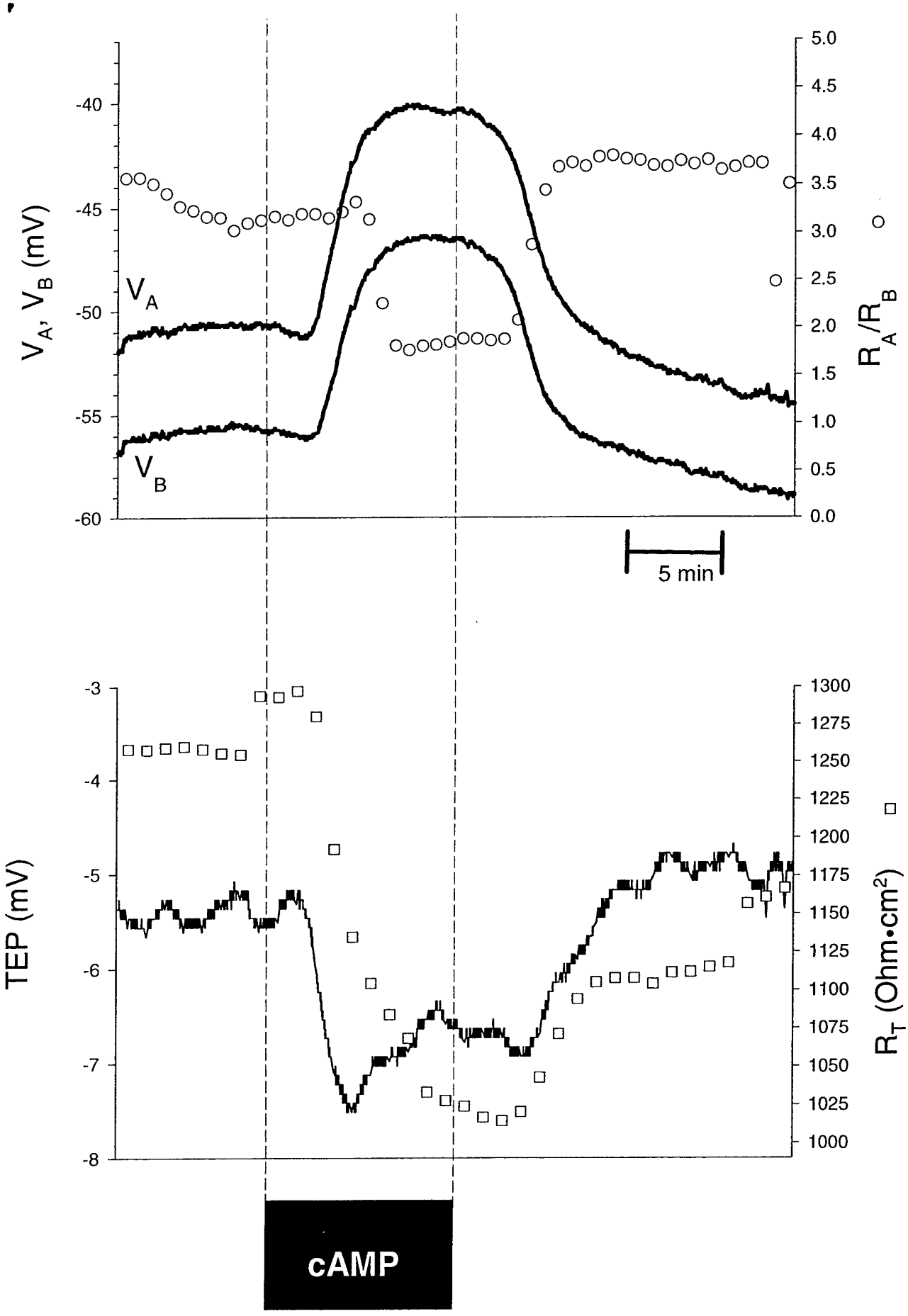
V_A, V_B (mV)
-40
-45
-50
-55
-60
V_A
V_B
5.0
4.5
4.0
3.5
3.0
2.5
2.0
1.5
1.0
0.5
0.0
R_A/R_B
5 min
TEP (mV)
-3
-4
-5
-6
-7
-8
1300
1275
1250
1225
1200
1175
1150
1125
1100
1075
1050
1025
1000
R_T (Ohm•cm^2)
cAMP

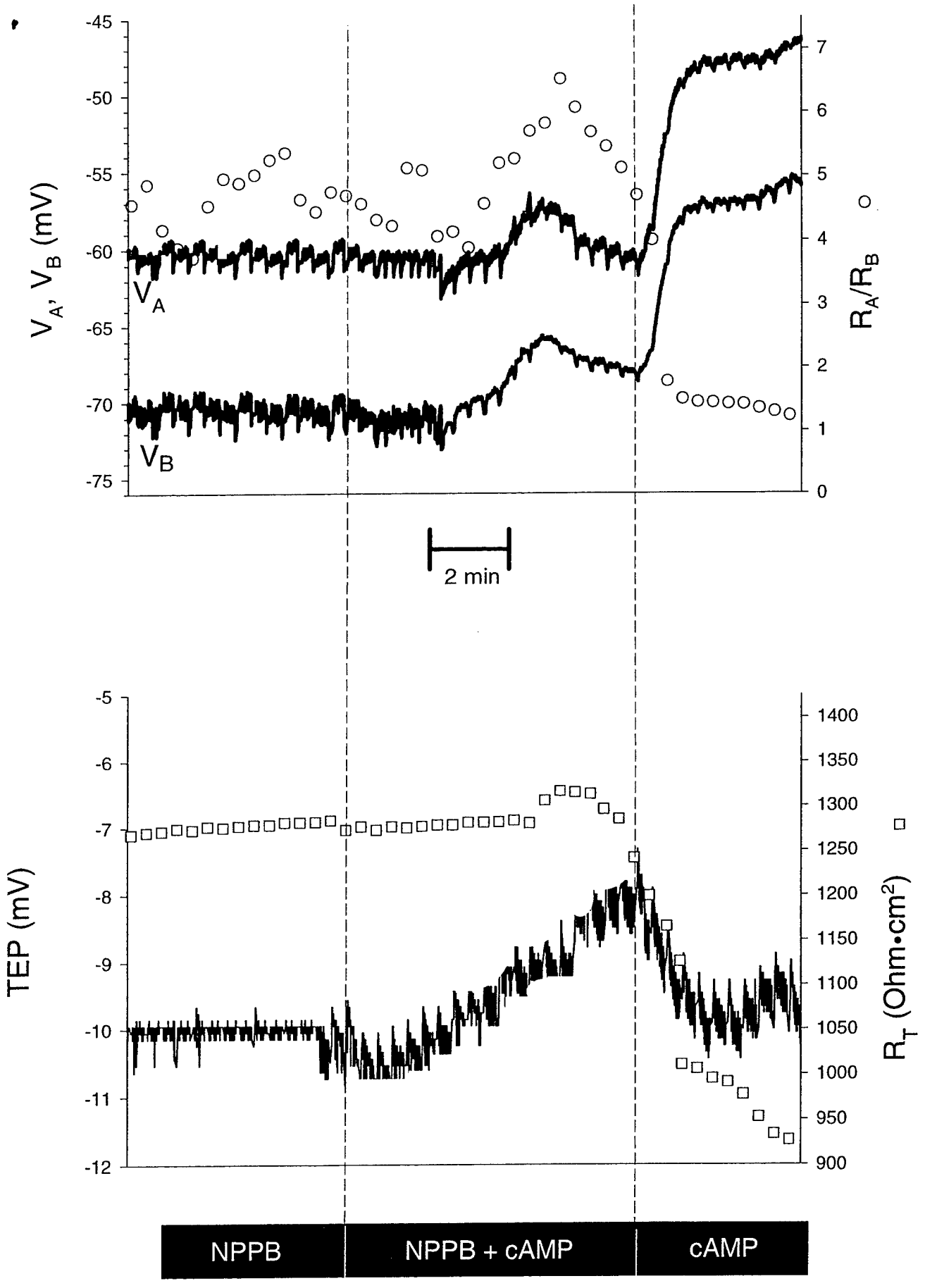
-45
-50
-55
-60
-65
-70
-75
V_A, V_B (mV)
V_A
V_B
7
6
5
4
3
2
1
0
R_A/R_B
2 min
-5
-6
-7
-8
-9
-10
-11
-12
TEP (mV)
1400
1350
1300
1250
1200
1150
1100
1050
1000
950
900
R_T (Ohm•cm^2)
NPPB
NPPB + cAMP
cAMP

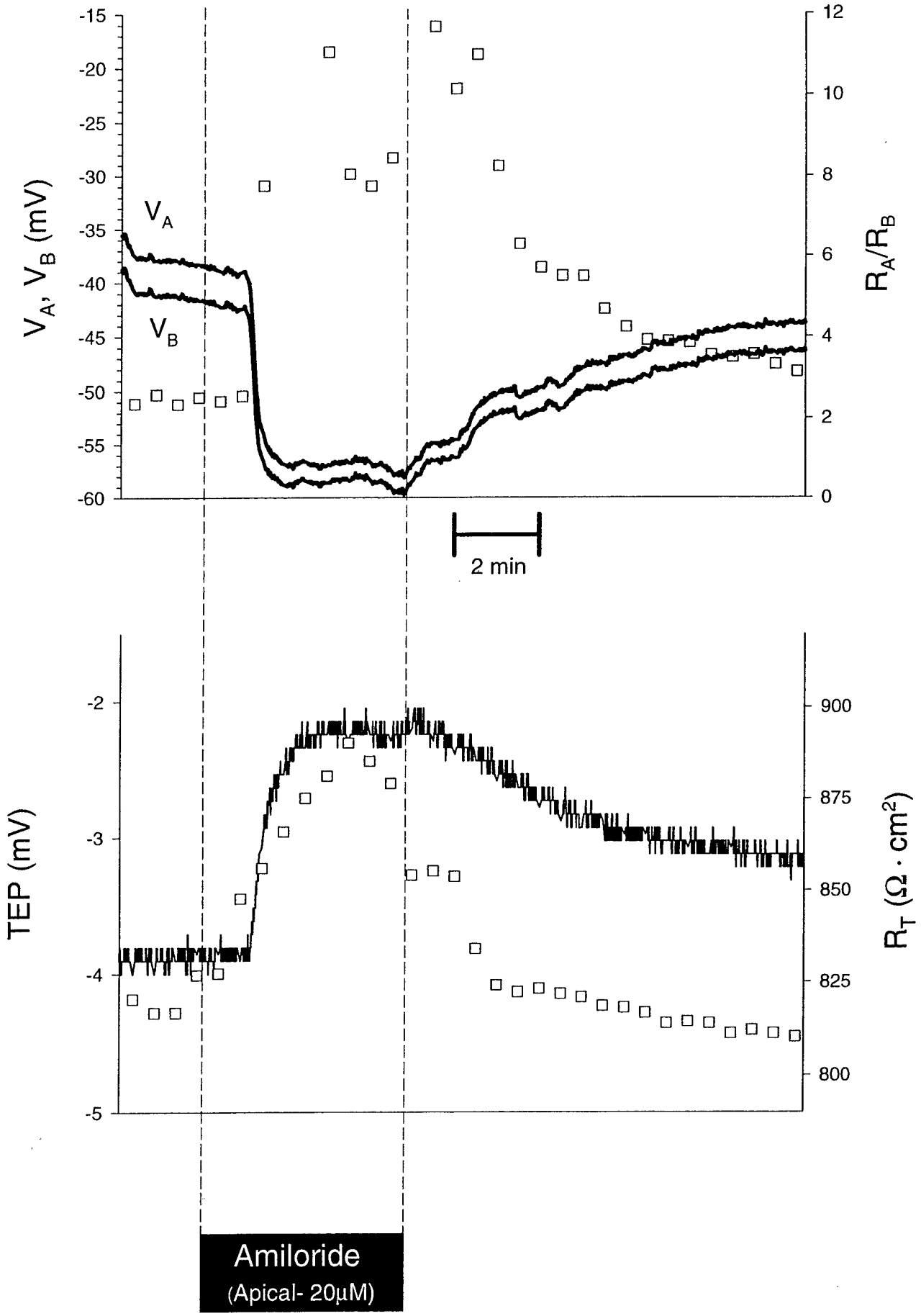
-15
-20
-25
-30
-35
-40
-45
-50
-55
-60
12
10
8
6
4
2
0
V_A, V_B (mV)
R_A/R_B
V_A
V_B
2 min
-2
-3
-4
-5
900
875
850
825
800
TEP (mV)
R_T ($\Omega \cdot cm^2$)
Amiloride
(Apical- 20μM)

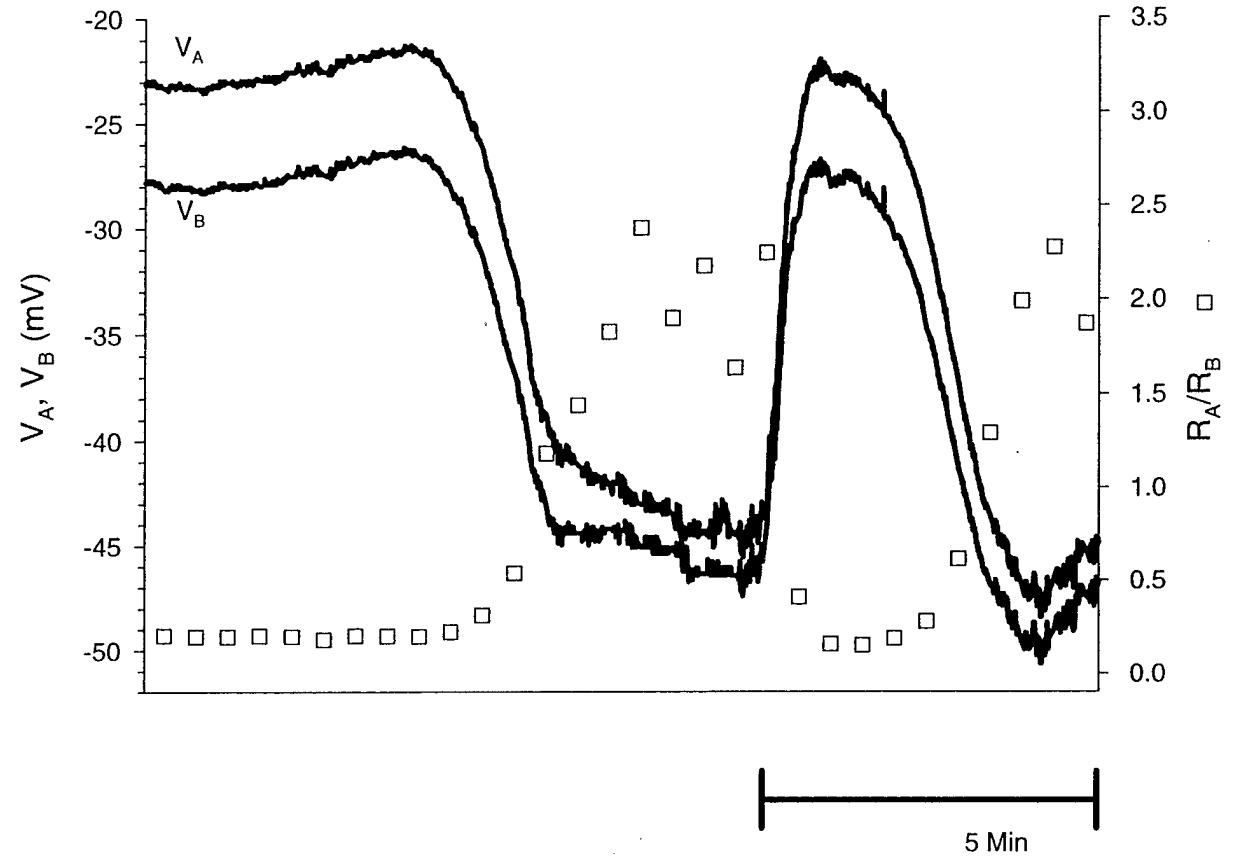

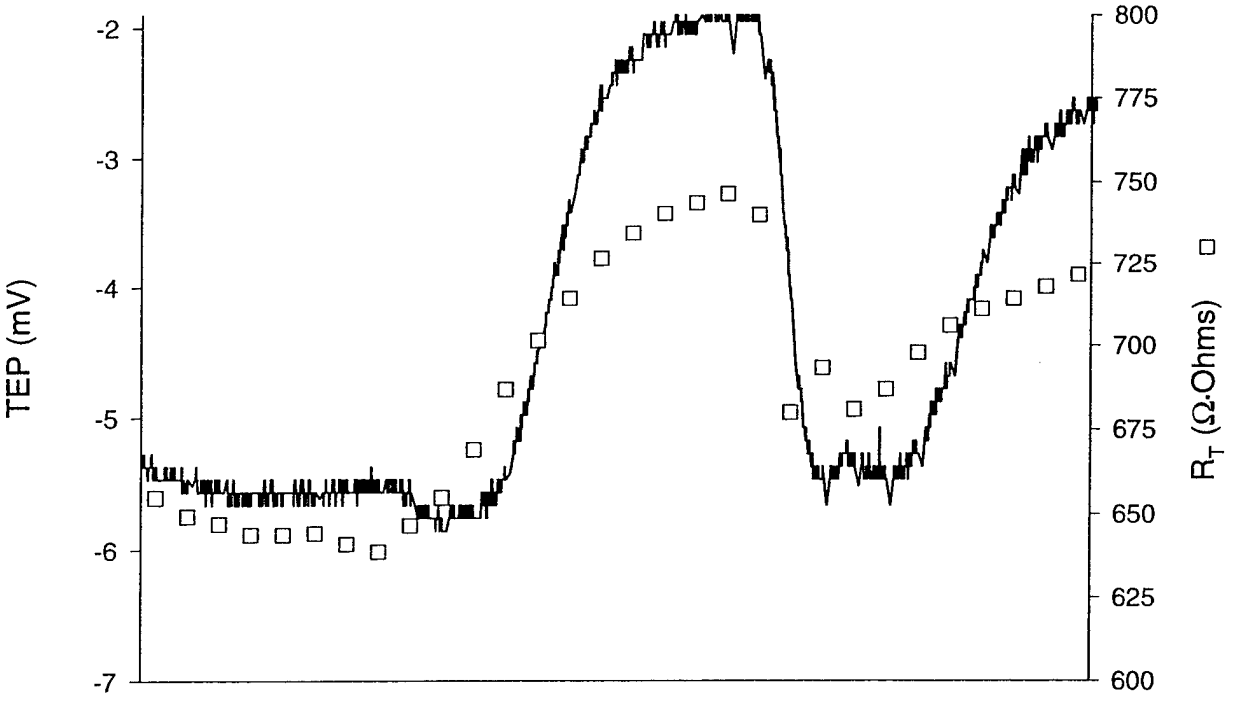

Amiloride

cAMP

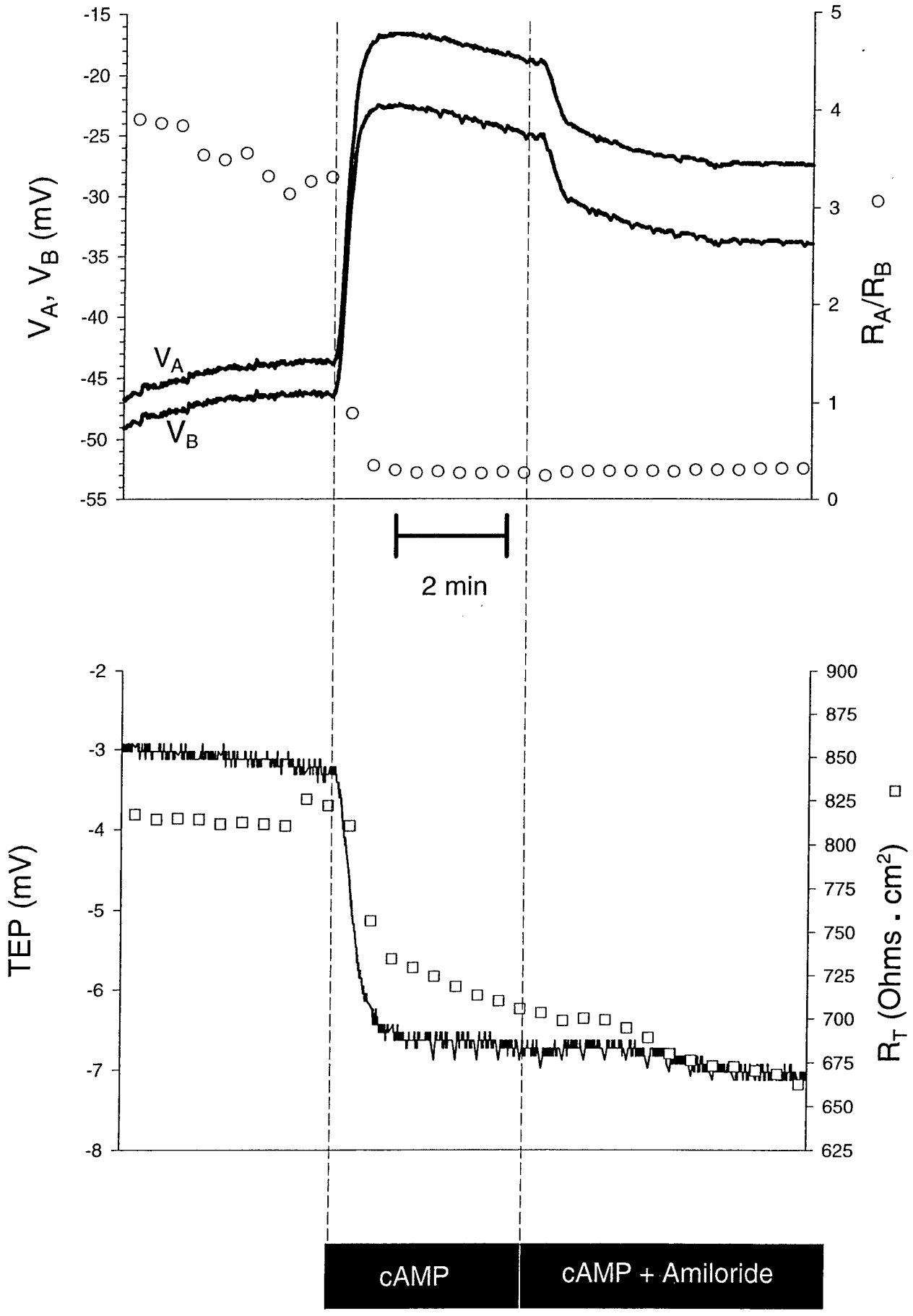
-15
-20
-25
-30
-35
-40
-45
-50
-55
5
4
3
2
1
0
V_A, V_B (mV)
R_A/R_B
V_A
V_B
2 min
-2
-3
-4
-5
-6
-7
-8
900
875
850
825
800
775
750
725
700
675
650
625
TEP (mV)
R_T (Ohms . cm^2)
cAMP
cAMP + Amiloride

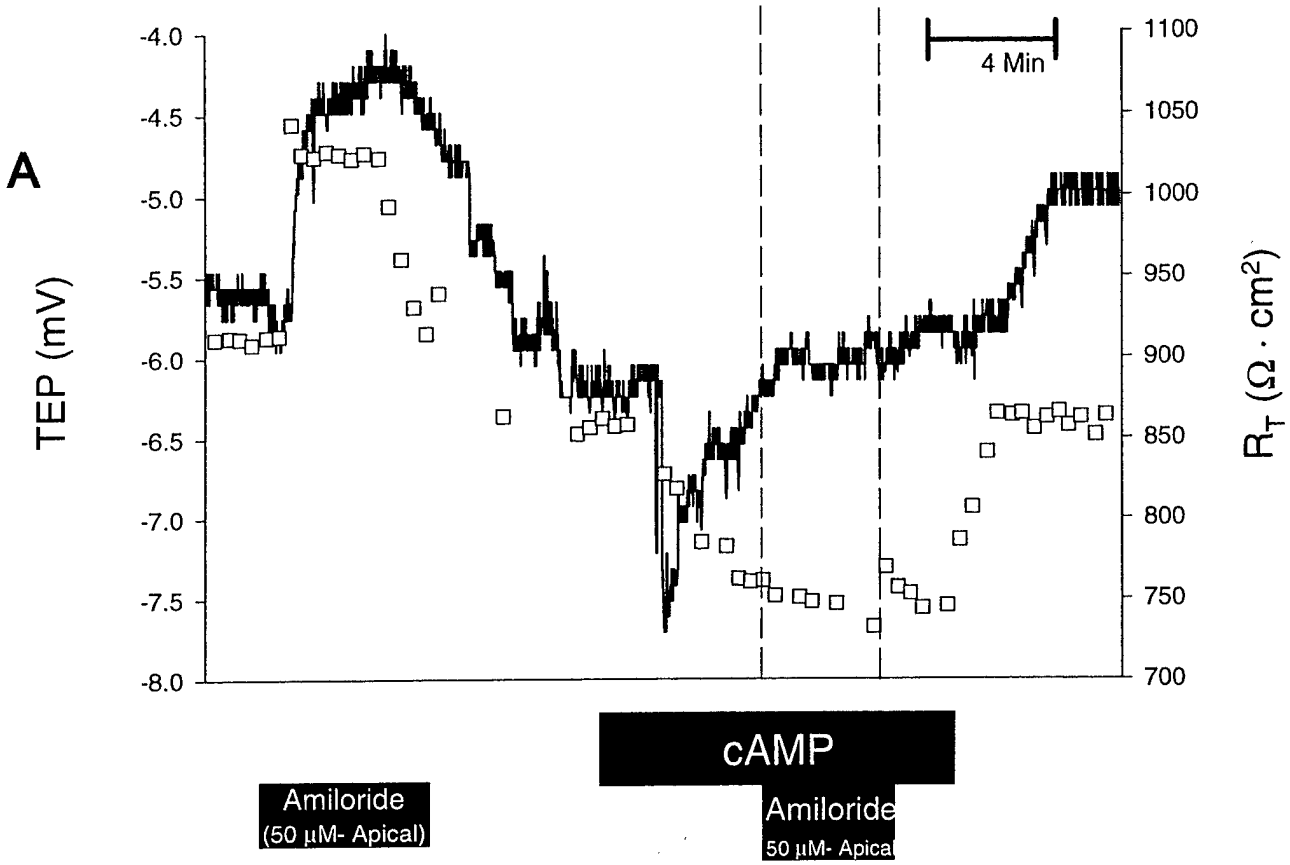
A
TEP (mV)
-4.0
-4.5
-5.0
-5.5
-6.0
-6.5
-7.0
-7.5
-8.0
4 Min
1100
1050
1000
950
900
850
800
750
700
R_T ($\Omega \cdot cm^2$)
cAMP
Amiloride
(50 µM- Apical)
Amiloride
50 µM- Apical

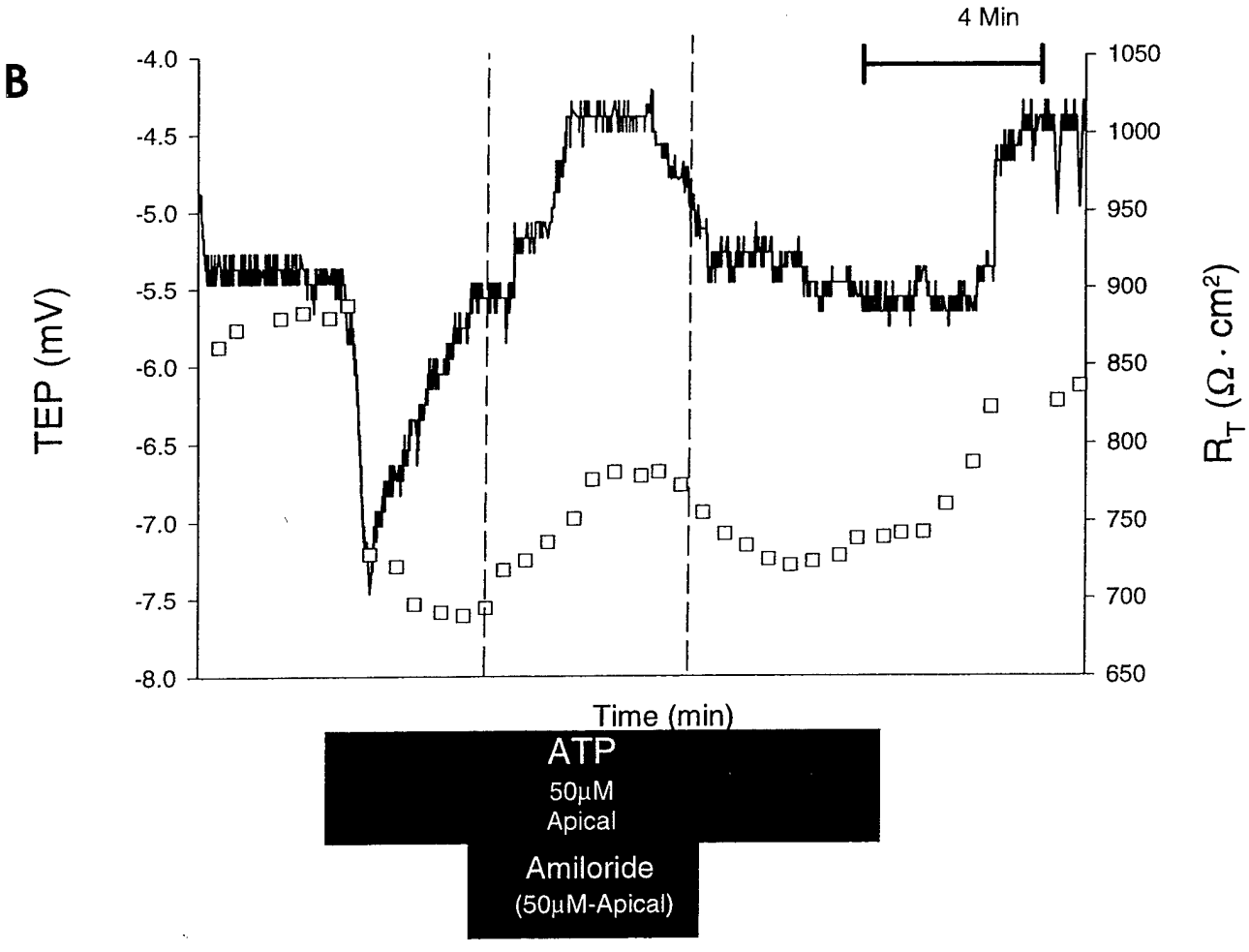
B
TEP (mV)
-4.0
-4.5
-5.0
-5.5
-6.0
-6.5
-7.0
-7.5
-8.0
4 Min
1050
1000
950
900
850
800
750
700
650
R_T ($\Omega \cdot cm^2$)
Time (min)
ATP
50µM
Apical
Amiloride
(50µM-Apical)

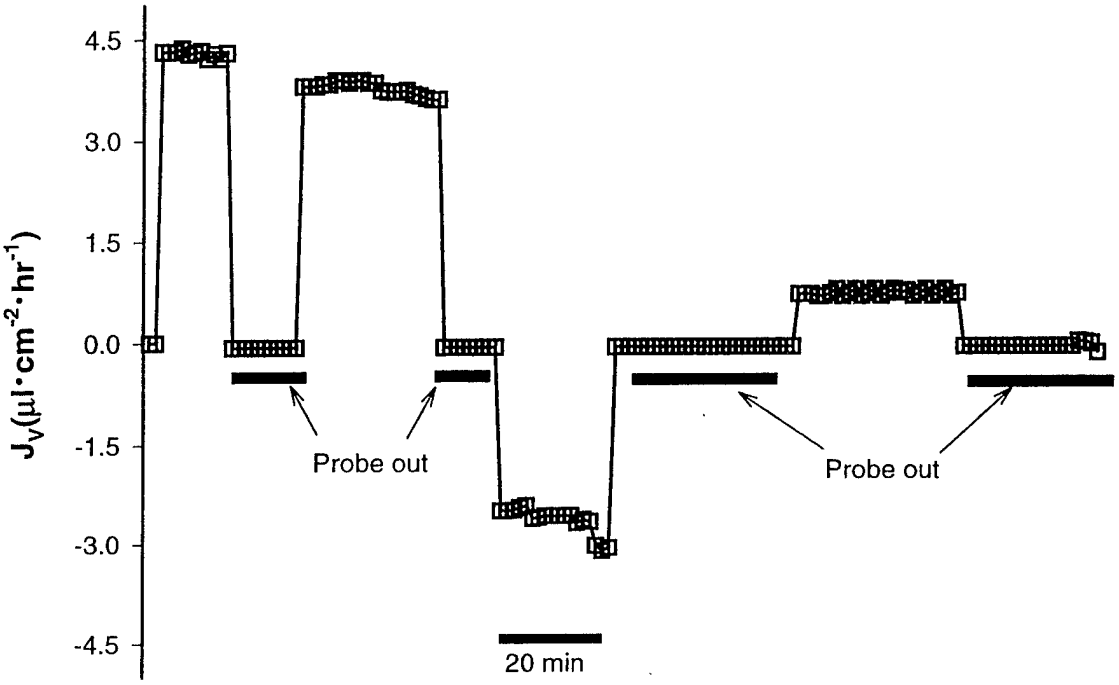
4.5
3.0
1.5
0.0
-1.5
-3.0
-4.5
$J_V(\mu l \cdot cm^{-2} \cdot hr^{-1})$
Probe out
Probe out
20 min

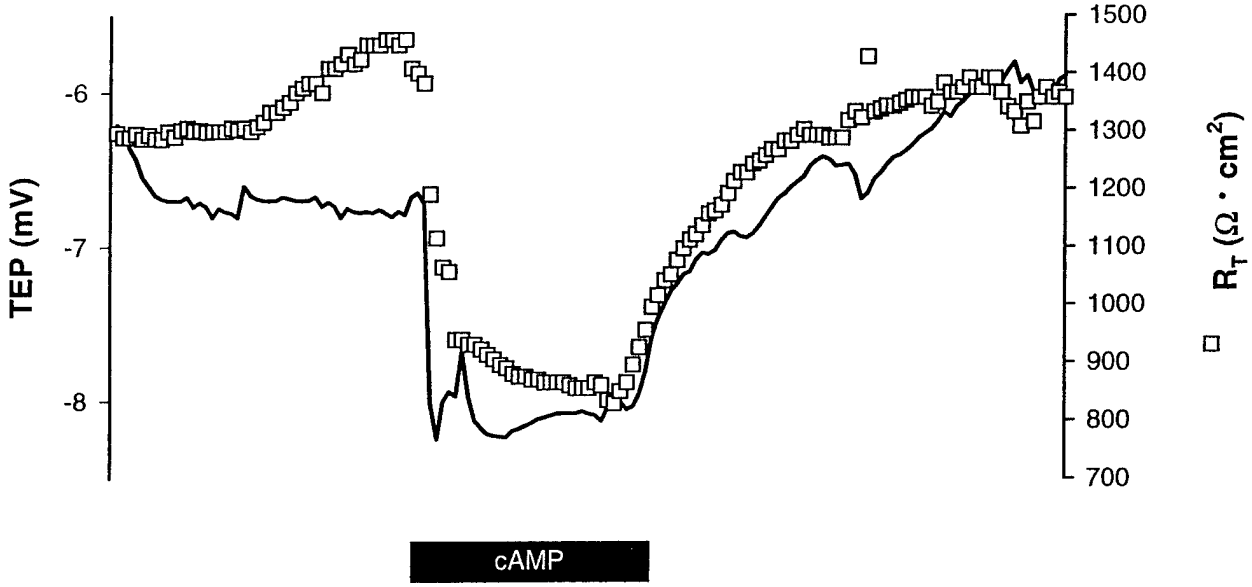
-6
-7
-8
TEP (mV)
1500
1400
1300
1200
1100
1000
900
800
700
R_T ($\Omega \cdot cm^2$)
cAMP

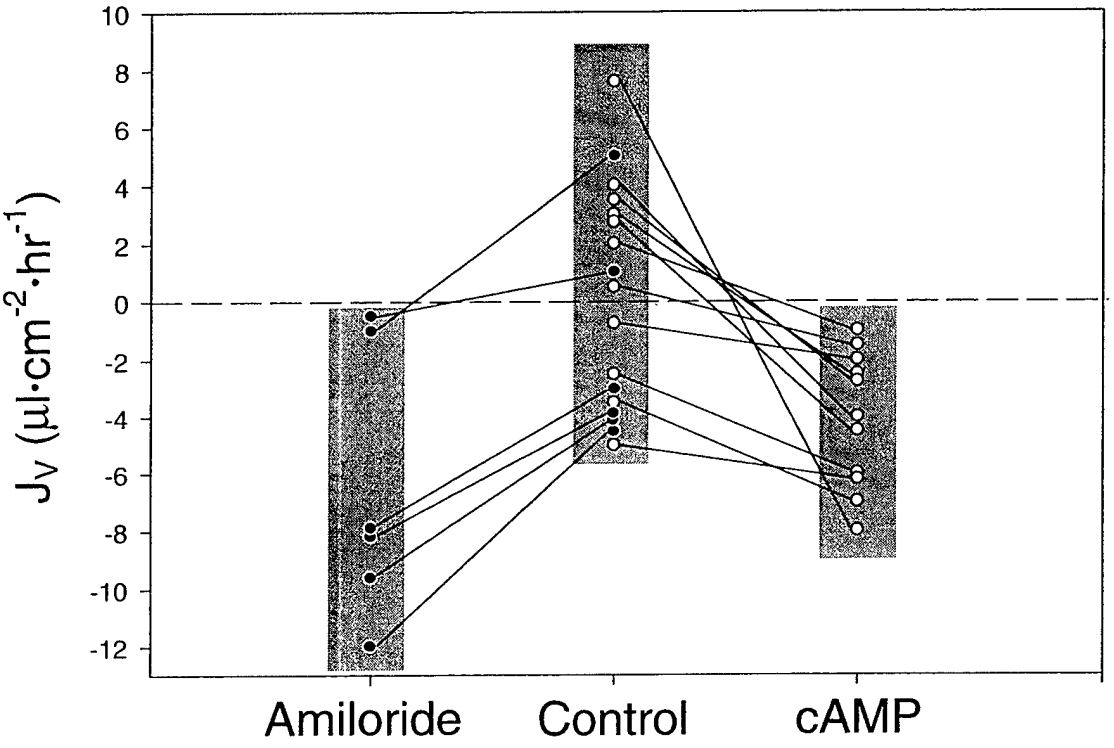
10
8
6
4
2
0
-2
-4
-6
-8
-10
-12
J_V (µl·cm^{-2}·hr^{-1})
Amiloride
Control
cAMP

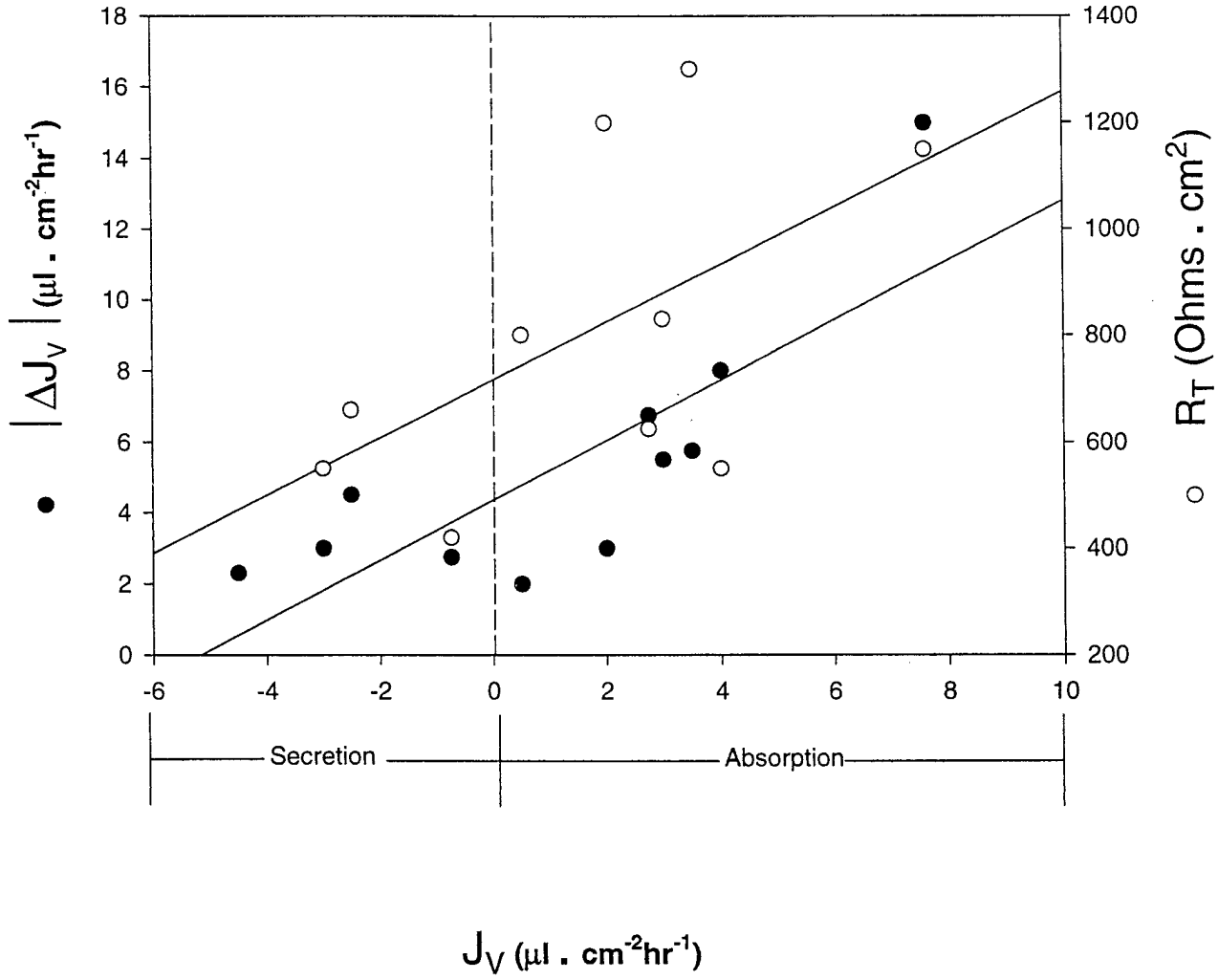
18
16
14
12
10
8
6
4
2
0
1400
1200
1000
800
600
400
200
-6
-4
-2
0
2
4
6
8
10
Secretion
Absorption
● |ΔJV| (µl . cm-2hr-1)
○ RT (Ohms . cm2)
JV (µl . cm-2hr-1)